INVESTIGATION OF MAGNETIC PARTICLE IMAGING:

LOCALIZATION ALONG ONE DIMENSION

A Thesis

by

JOSHUA WENTAU LIAOU

Submitted to the Office of Graduate and Professional Studies of
Texas A&M University
in partial fulfillment of the requirements for the degree of

MASTER OF SCIENCE

Chair of Committee,	Steven M. Wright
Committee Members,	Robert Nevels
	Jim Ji
	Corey Bishop
Head of Department,	Miroslav Begovic

May 2019

Major Subject: Electrical Engineering

ABSTRACT

Magnetic particle imaging (MPI) is a novel tracer-based imaging modality that was first introduced in 2006. MPI utilizes the unique magnetic properties of super paramagnetic iron oxide nanoparticles (SPIONs) to produce temporospatial information. In addition, MPI has the potential for high resolution and high sensitivity.

The main components of MPI can be broken down into the transmit signal chain and the receive signal chain. This research project will discuss some of the basic concepts behind MPI in addition to explaining some of the practical hardware designs and considerations in an MPI system. There is a section on debugging the hardware and software as this was a major component of the project. This section mainly identifies the noise sources in addition to presenting a guide and tips on how to decouple the transmit coil and receive coil. The section on tests and results analyzes the specification of the MPI system by characterizing the gradient coil, analyzing the detection limit for the relaxometry component of the system, and the sensitivity and resolution of the 1D MPI system.

The objective of the project is to design and build a 1D MPI system that is portable and cost-effective with a resolution that would be suitable for imaging.

DEDICATION

For future aspiring MPI researchers, hopefully this will help you through some growing pains.

ACKNOWLEDGEMENTS

I would like to thank my committee chair, Dr. Steven Wright, for his guidance throughout my graduate studies, teaching me how to think critically and methodically, and providing direction in my research.

In addition, I would like to express my gratitude to my committee members, Dr. Robert Nevels, Dr. Corey Bishop, and Dr. Xiaoning Qian for providing their expertise and time.

I would like to thank my father and mother, Kuo and Meei, for their encouragement and assistant. I would not be where I am today without them.

Finally, I would like to thank my wife, Yashmeena, for her patience and love. Without her support, I would not have been able to pull through. She was with me when I needed her the most.

CONTRIBUTORS AND FUNDING SOURCES

Contributors

This work was supervised by a thesis committee consisting of Professor Steven Wright and Professors Robert Nevels and Jim Ji of the Department of Electrical and Computer Engineering and Professor Corey Bishop of Biomedical Engineering.

Nick Fortune made contributions in multiple areas of the thesis in particular the coil fixture design and coil fabrication.

Funding Sources

My research was supported through Professor Steven Wright's discretionary funds.

TABLE OF CONTENTS

PAGE

LIST OF FIGURES

Page

LIST OF TABLES

Page

CHAPTER I

INTRODUCTION

I.1 Thesis Overview

This thesis will be subdivided into four main categories: introduction, magnetic particle imaging hardware, system debugging, test and results, and future works.

The introduction chapter will provide a brief overview of MPI in addition to some basic theory relevant to MPI such as the nanoparticles, the gradients, and the signal spectrum.

The magnetic particle imaging hardware chapter will cover the major hardware components of MPI such as the transmit chain, receive chain, the gradient coil, and nanoparticles. In this section, the LabVIEW program will be discussed as well.

The system debugging chapter will analyze the system and debug some potential noise sources. Some of the major sources of noise identified were the signal processing in a LabVIEW VI and the transmit coil and receive coil coupling from the MPI system. In addition, the gradient strength was characterized in this section.

The test and results chapter will first discuss the proof of particles. In this section, a couple experiments will be performed to show that the signal from the receive coil is from detecting the particles rather than from coupling the transmit coil and receive coil due to a change in the magnetic environment from introducing a metal object.

The future works chapter covers potential next steps for the MPI project. Some of the items discussed were lowering the noise baseline, modifying the gradiometer design, and improving the gradient system.

I.2 Magnetic Particle Imaging Introduction

The first paper published on magnetic particle imaging (MPI) was in 2005 by Gleich and Weizenecker, just a little over ten years ago [1]. Since then, MPI has gained traction as a new medical imaging modality that would offer physicians new diagnostic and therapeutic options. By 2008, just three years later, Weizenecker et.al. published research on three-dimensional real-time in vivo magnetic particle imaging [2]. Although there has yet to be a human scanner, MPI is in a similar stage to where MRI was in the early 1980s and has the potential to impact the medical field just like MRI has today.

Since MPI is a non-ionizing tracer-based imaging modality, it has the potential to provide novel and crucial information in addition current imaging systems. While computed tomography (CT) scans can use tracers, the radiation energy is harmful to the patients. MRI does not utilize radiation energy that is harmful to patients; however, it has limitation and is subject to image artifacts. While MPI does not replace these two imaging techniques, it does provide information where the other two imaging techniques have difficulty providing. MPI provides great contrast in addition to zero depth attenuation due to low-frequency magnetic fields [3]. Currently, MPI has shown the most promise in angiographic and stem-cell tracking applications [4].

I.3 Magnetic Particle Imaging Overview

Magnetic particle imaging utilizes the unique magnetization response of superparamagnetic iron oxide nanoparticles (SPIONs), in addition to manipulating magnetic fields to elicit a detectable signal. Before diving further into the MPI phenomenon, a few terminologies need to be defined, namely the transmit coil, the receive coil and the gradient coil.

An oscillating magnetic field produced by a coil is used to flip the magnetization of the particles in MPI. This oscillating magnetic field is sometimes called the modulation field and/or the excitation field [1],[4]. In this paper, this oscillating magnetic field will be called the excitation field, the frequency of the excitation field will be called the excitation frequency or fundamental frequency, and the coil that produces the excitation field will be called the transmit coil.

While the SPIONs are exposed to the excitation field, the magnetization direction of the SPIONs will change with direction of the magnetic field produced by the excitation field. The change in magnetization is then picked up by a coil. Based on Faraday's law, a change in magnetization will produce a corresponding voltage signal. This coil is called the receive coil.

In addition to the transmit coil and the receive coil, there is the gradient coil, also known as the selection field [5]. A magnetic gradient field is a change in magnetic field as the spatial position changes. A gradient coil is composed of two coil that having windings in opposite directions. The gradient coil provides spatial information which will be further discussed in this section.

Now that the three main coils have been briefly discussed, we will go into the phenomenon of MPI. As mentioned before MPI uses the transmit coil to produce an oscillating magnetic field. The SPIONs have a unique magnetization response that emulate a Langevin function. An oscillating magnetic field produced by the transmit coil will cause the direction of the magnetization response of the SPIONs to flip. The SPION magnetization response will change with time in accordance to the magnetic field generated by the transmit coil. The change of the magnetization response is picked up by the receive coil. By taking the Fourier transform of the magnetization response, the fundamental frequency of the excitation field is seen in addition to its harmonics. In MPI, the fundamental frequency and the harmonics are the basic signal to producing an image.

At this point with only the transmit coil and the receive coil, the signal is coming from every SPION at every position within the receive coil. There is currently no spatial information. To extract spatial information from the SPIONs, a gradient is used to superimpose an additional magnetic field on the excitation field to force the magnetization of the SPIONs in the saturation region. As discussed in the previous paragraph, the nanoparticles have a Langevin response. This means that there is a dynamic region, where the magnetization rapidly changes to an external magnetic field, and there is a saturated region, where the magnetization does not change much to the external magnetic field. If the SPIONs are exposed to a oscillating magnetic field that causes the particles to oscillate in the saturated region, the Fourier transform of the

magnetization response will show very little fundamental and harmonic signals as seen in the spectrum plot.

I.4 Superparamagnetic Iron Oxide Nanoparticles

Superparamagnetic iron oxide nanoparticles (SPIONs) are a fundamental component in MPI. SPIONs are composed of an iron oxide core with a biocompatible nonmagnetic polymer coating. The SPION magnetization will follow the direction of the applied magnetic field. This is also known as Neel rotation [6]. Neel rotation describes the rotation of the particle due to its magnetic moment. In addition to particle rotation due to the magnetic moment (Neel), there is also the mechanical rotation of the particle, which is known as Brownian rotation. The excitation field can cause both Neel and Brownian rotation.

The unique characteristic of SPION magnetization can be characterized with the Langevin function [6]. The Langevin function is described as

$$\mathcal{L}(\xi) := \begin{cases} (\coth(\xi) - \frac{1}{\xi}, & \xi \neq 0 \\ 0, & \xi = 0 \end{cases} \quad (1)$$

The SPION magnetization response to an external magnetic field is described by the following equation:

$$M(H) = cm\mathcal{L}(\beta H) \quad (2)$$

With

$$\beta = \frac{\mu_0 m}{k_b T^P} \quad (3)$$

Where c represents concentration, μ_0 represents the permeability of free space, m represents the modulus of the magnetic moment of a single particle, k_b represents the Boltzmann constant, and T^P represents the particle temperature [6].

The magnetic moment, m, can be described with the following equation:

$$m = VM_{core}^{s} \tag{4}$$

Where V represents the volume of the SPIONs and M_{core}^{s} represents the saturation magnetization of the SPIONs. MATLAB () was used to simulate the particle magnetization response to an applied magnetic field. The results are shown in Figure 1.

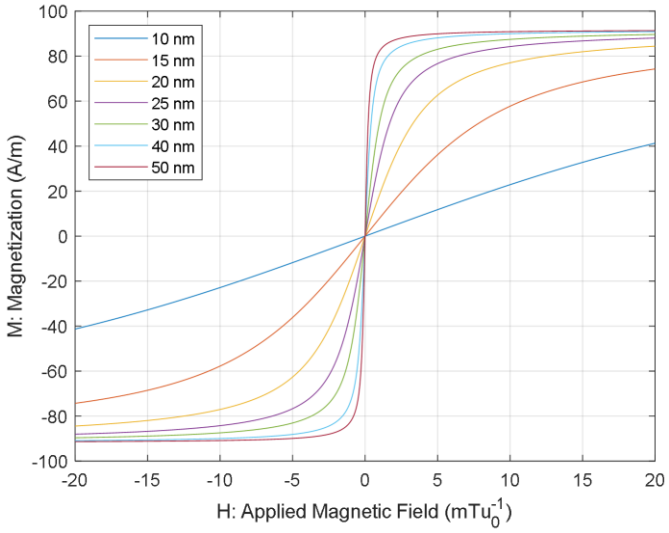

Figure 1. Magnetization response of SPIONs to an applied magnetic field.

The resolution of the SPIONs is derived from taking the derivative of the magnetization in response to the applied magnetic field (dM/dH) and defined as the full-width at half max (FWHM) [6] . The derivative of the Langevin function is described by the following equation [6]:

$$\mathcal{L}'(\xi) := \begin{cases} \left(\frac{1}{\xi^2} - \frac{1}{\sinh^2(\xi)}\right), & \xi \neq 0 \\ \frac{1}{3}, & \xi = 0 \end{cases} \quad (5)$$

The derivate of the magnetization response in respect to an applied magnetic field is shown in the middle plot in Figure 2. The derivative of the magnetization results in a point spread function (PSF). Therefore, dM/dH peaks in the middle and gradually decreases as the SPIONs experiences an increasing/decreasing applied magnetic field. By introducing a gradient field to the nanoparticles, the resolution of the nanoparticles was defined as FWHM as shown in the bottom plot in Figure 2. The gradient field will be further discussed in Section I.5.

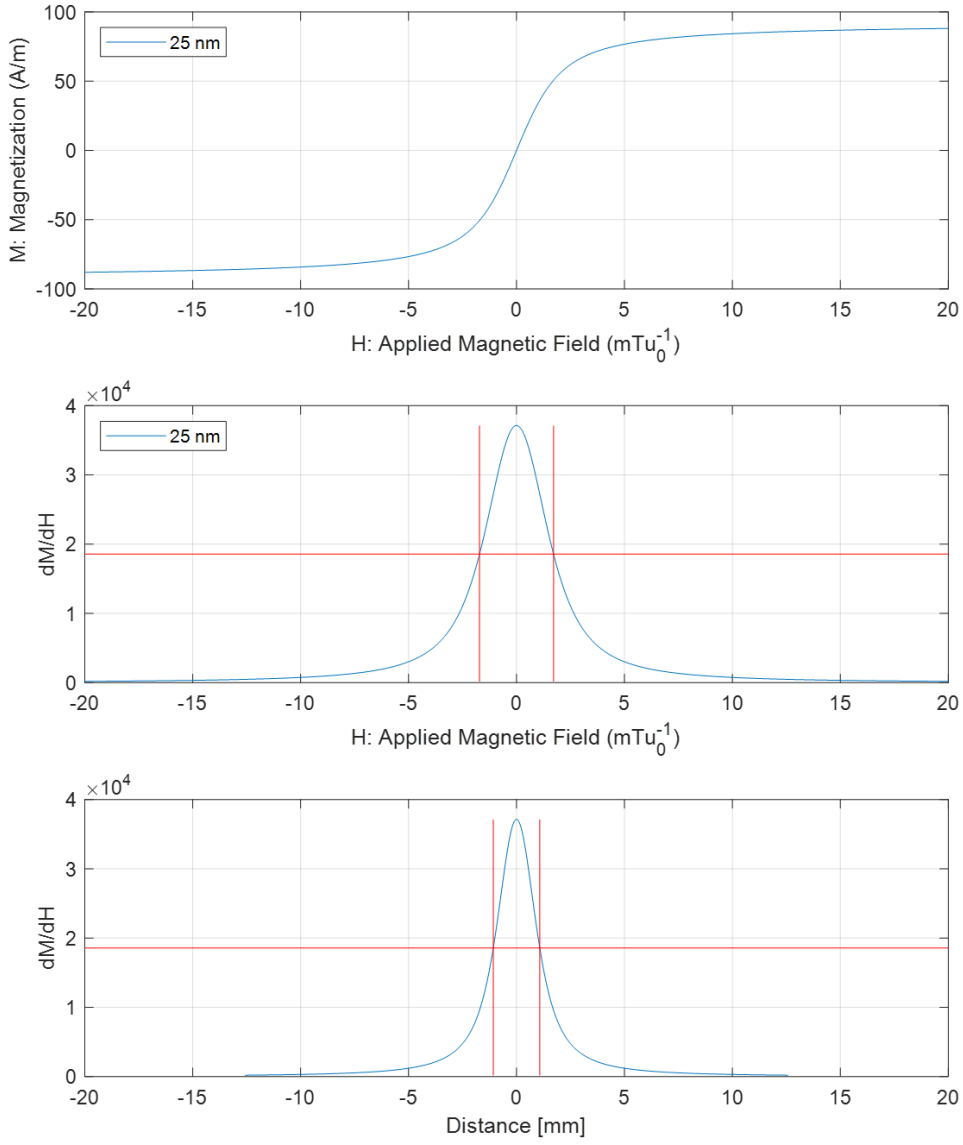

Figure 2. (Top) Magnetization response of 25 nm SPIONs in response to magnetic field. (Middle) The derivative of the top plot. It displays the change in magnetization as a function of the applied magnetic field. (Bottom) Converts the applied magnetic field to position when a 2 T/m gradient strength is applied. Simulation with 25 nm SPIONs, 2 T/m gradient strength

In addition to defining resolution, another key aspect is defining saturation of the nanoparticles. Saturation field strength (H^s) is defined as 80% saturation of the

nanoparticles [6]. Therefore, by setting $\mathcal{L}(\xi)$ = 0.8, ξ^s is approximately equal to 5 as seen in Figure 3.

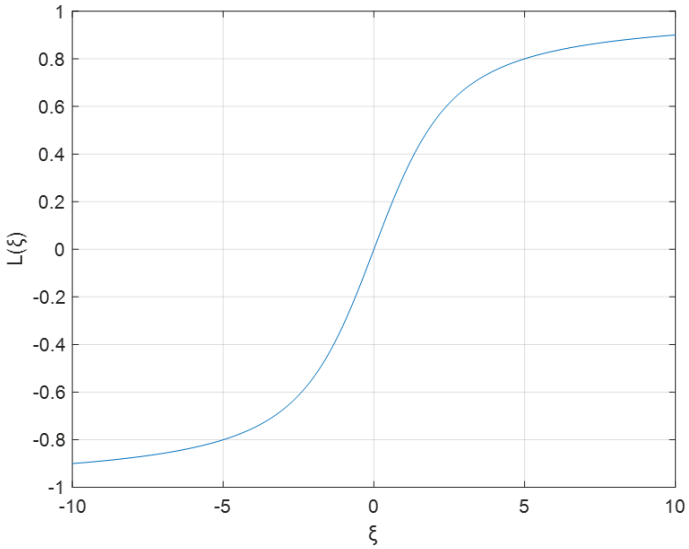

Figure 3. Plot of the Langevin function. For MPI, saturation is when $\mathcal{L}(\xi)$ = 0.8.

Therefore,

$$\xi^s = 5 = \beta H^s \tag{6}$$

Therefore, H^s is defined as the following:

$$H^s = \frac{5k_bT^P}{\mu_0 m} \tag{7}$$

The saturation of the particles is determined by the size of the particle which is an inherent property of the magnetic moment, m. Therefore, as the particle size increase, the applied magnetic field strength decreases for the nanoparticles to reach saturation.

I.5 Gradient

Without a magnetic gradient, there would be no spatial information regarding the location of the nanoparticles. A magnetic gradient, or the selection field, is essentially a change in the magnetic field as position changes. For example, if the magnetic field changes from -1 T to 1 T over 2 meters, the magnetic gradient strength would be 1 T/m. The central position would experience little to no magnetic field which is also known as the null point or null region. An example of the magnetic field produced by a gradient is shown in Figure 4.

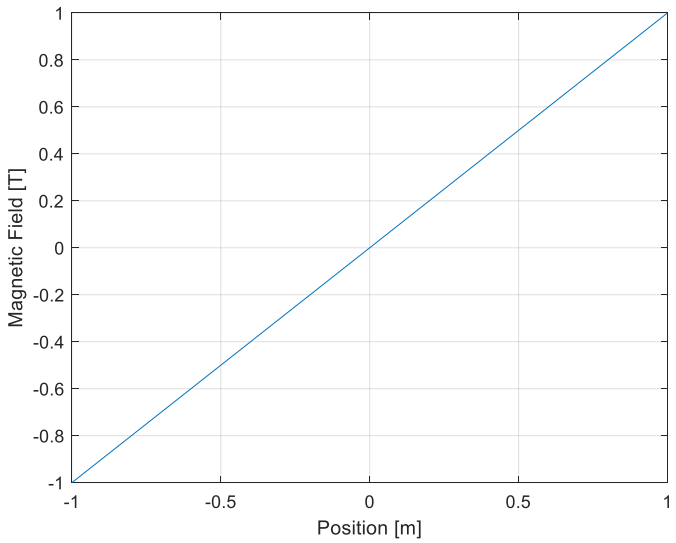

Figure 4. Plot of magnetic field vs. position. For this magnetic field distribution with distance, the gradient strength would be 1 T/m

As discussed in Section I.3, by applying an oscillating magnetic field, the magnetization response of the SPIONs will change. Although the magnetization response can be detected, there is no spatial information related to the signal without the gradient. By superimposing a magnetic gradient field on the region, the particles near the

center of the gradient field will respond to the oscillating magnetic field; however, the particles move away from the center of the gradient field, they will have less change in their magnetization response.

When an external magnetic gradient field is applied to the nanoparticles, there is little change in the magnetization of the particles. As a result, the particles that experience this magnetic field will not produce any particle signal. However, the particles in the dynamic region will respond to the applied magnetic field.

For each additional dimension, there will need to be an additional set of gradients. Therefore, for 1D imaging, there will need to be one set of gradients, and for 3D imaging, there will need to be three sets of gradients, one for each axis.

I.6 Signal Spectrum

Since the excitation field is periodic, the induced nanoparticles signals will also be periodic. Using the Taylor series to expand the Langevin function, the generation of the higher harmonics can be mathematically described with the following equation:

$$\mathcal{L}(\xi) = \frac{1}{3}\xi - \frac{1}{45}\xi^3 + \frac{2}{954}\xi^5 - \frac{1}{4725}\xi^7 + \cdots \quad (8)$$

If the arguments $\xi = \frac{\mu_0 m}{k_b T^P} H$, $H = -A^E cos(2\pi f^E t)$, and $\xi = \tilde{\xi}\cos(2\pi f^E t)$ where $\tilde{\xi} = -\frac{\mu_0 A^E m}{k_b T^P}$ are applied to the Langevin function, then the nanoparticles magnetization response can be described as the following equation:

$$\mathcal{L}\left(\tilde{\xi}\cos(2\pi f^E t)\right) = \frac{1}{3}\tilde{\xi}\cos(2\pi f^E t) - \frac{1}{45}\widetilde{\xi^3}(\cos(2\pi f^E t)^3 + \cdots \quad (9)$$

Using the identity formula:

$$\cos^3(x) = \frac{1}{4}(3\cos(x) + \cos(3x)) \tag{10}$$

Then the equation becomes:

$$\mathcal{L}\left(\widetilde{\xi}\cos(2\pi f^E t)\right) = \frac{1}{3}\widetilde{\xi}\cos(2\pi f^E t) - \frac{1}{60}\widetilde{\xi^3}(\cos(2\pi f^E t)^3 + \cdots$$

$$= \frac{20\widetilde{\xi} - \widetilde{\xi}^3}{60}\cos(2\pi f^E t) + \frac{\widetilde{\xi}^3}{180}\cos(2\pi(3f^E)t) + \cdots \tag{11}$$

Therefore, by including $\cos^5$, $\cos^7$, …, and so forth, one can mathematically determine that all the odd harmonics are present in the signal spectrum [6] with most of the signal content being in the excitation field and third harmonic [7].

I.7 Magnetic Particle One Dimensional Imaging

In this project, a 1D MPI system will be discussed, developed, and demonstrated. The 1D MPI system begin as a magnetic particle relaxometry, which consist of the transmit coil and receive coil without the gradient coil. Once the relaxometry portion has been characterized, the gradient coil will be incorporated into the system, making it a 1D MPI system. Since this project attempts a 1D system, the system will only require one gradient set.

I.8 Excitation Frequency/Fundamental Frequency

Recently, MPI researchers have been trying to recover the particle signal from the excitation frequency [8]. Previously, most groups have focused on the third harmonic, since it is the first available harmonic to contain a pure signal from the particles without disruption from the excitation field [9]. However, by filtering and

disregarding the fundamental frequency, a significant portion of the MPI signal is lost. Therefore, a key component to improve the MPI signal is figuring out a method to null the excitation field from the signal coming into the receive coil. In this project, we will attempt to null out the excitation field in an attempt to preserve the fundamental frequency using a gradiometer configuration as the receive coil [8]. More about the receive coil design will be discussed on Section II.3.

I.9 Project Aims

In addition to electrical and mechanical engineering consideration inherent to this project, the design choices of the hardware were determined by a few factors. Each component of the project had the following goals in mind:

(1) Physical dimensions relevant to small mouse/rat imaging. A wistar rat length can range from 12 cm to 22 cm [13] and width of a minimum of approximately 3 cm [15].

(2) Detection limit that would have some clinical relevance. The target concentration is approximately $4 \times 10^4 \ \frac{particles}{mm^3}$. This will be discussed further in Section II.5.2.

(3) Resolution suitable for small animal imaging.

(4) Portable MPI system

The overall goal of the research project is to develop a 1-D MPI system, thereby demonstrating the potential of MPI in medical diagnostics through phantom studies.

Aim 1 — Design a magnetic particle relaxometer (MPR**)**: The first step to designing an MPI system is to develop the signal chain. In other words, it is to develop

the MPI without the gradient. The signal chain will consist of two main components: the transmit chain and the receive chain. The purpose of the signal chain is to excite the particles through the transmit chain and then acquire the magnetic response of the nanoparticles through the receive chain.

Aim 2 — Design the gradient set: The gradient is one of the main determining factors of the resolution and speed of the MPI system. The purpose of the gradient is to provide a field free region (FFR) while providing a magnetic field that would saturate the magnetization of the particles outside of the FFR. For this project, only one gradient set will be used, therefore, the gradient will produce a field free plane (FFP). The gradient set will be designed using coils. Some major considerations for designing gradient coils are the wire size, wire shape, the fusing current of the wire, coil size, coil radius, and the current. Our goal is to produce a 2 mT/mm gradient strength in order to achieve a 2 mm resolution with 20 nm particles. An in-depth analysis of the gradient will be discussed in Section 0.

Aim 3 — Construct gradient to perform 1D scan: The MPI image can be constructed using two methods: a mechanical approach and an electronic approach. The mechanical approach is performed by moving the FFP through a mechanical process. The electronic approach is performed by changing the current through the gradients to move the FFP while the object is fixed. Each approach has its own advantages and disadvantages which will be discussed later in the research approach section.

Aim 4 — Characterize the MPI system: The MPI system will need to be characterized once it is constructed. The MPI system will be characterized in terms of its

resolution, speed, and sensitivity. In addition, various coil designs (e.g. gradient, receive coil, transmit coil) may be examined to optimize the MPI system. The characterization of the MPI system will be performed through using various phantom shapes and particle sizes. A reported SPIONs concentration well tolerated humans was approximately $70\,\frac{\mu mol\ Fe}{L}$ which translates to $2.1\ \times 10^{13}\,\frac{particles}{mm^3}$ or $0.0056\,\frac{mg}{ml}$ [11]. Currently, Conolly's MPI research group in Berkeley have published a sensitivity of $0.2\,\frac{\mu mol*Fe}{L}$ which translates to $372.5\ \frac{particles}{mm^3}$ or $1.6\ \times 10^{-5}\,\frac{mg}{mL}$ [12] which is well below the concentration limit. We will start off with a target sensitivity of the system will be approximately $20\,\frac{\mu mol*Fe}{L}$, which is an order of magnitude larger than the Berkeley's group. This translates to approximately $4\ \times 10^{4}\ \frac{particles}{mm^3}$ or $1.6\ \times 10^{-3}\,\frac{mg}{mL}$. The SPION concentration conversion equations will be discussed in Section II.5.2.

To summarize, our goal is to design a portable 1D MPI system with physical dimensions suitable for small mouse/rat imaging with a gradient strength of 2 mT/mm, a resolution of 2 mm, and a sensitivity of $4\ \times 10^{4}\ \frac{particles}{mm^3}$.

CHAPTER II

MAGNETIC PARTICLE IMAGING HARDWARE

II.1 Hardware Overview

Magnetic particle imaging can be broken down into the transmit chain and the receive chain. The transmit chain consists of the signal source, pre-amplifier, high power low pass filter, the matching/tuning network, and the transmit coil. The receive coil chain consists of the receive coil, the LNA, and the digitizer.

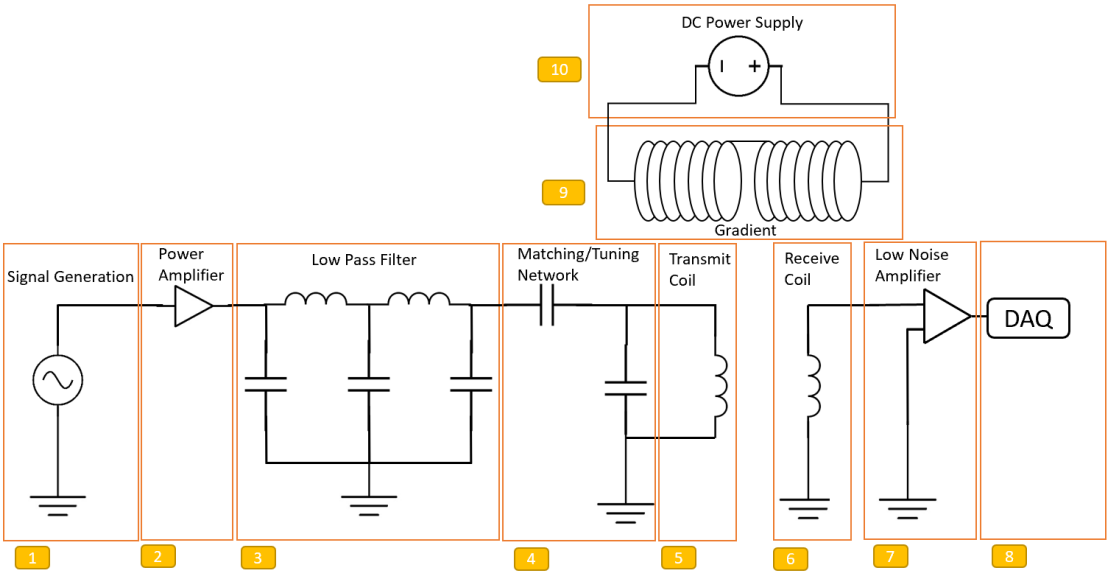

Figure 5. Schematic of the main components of MPI.

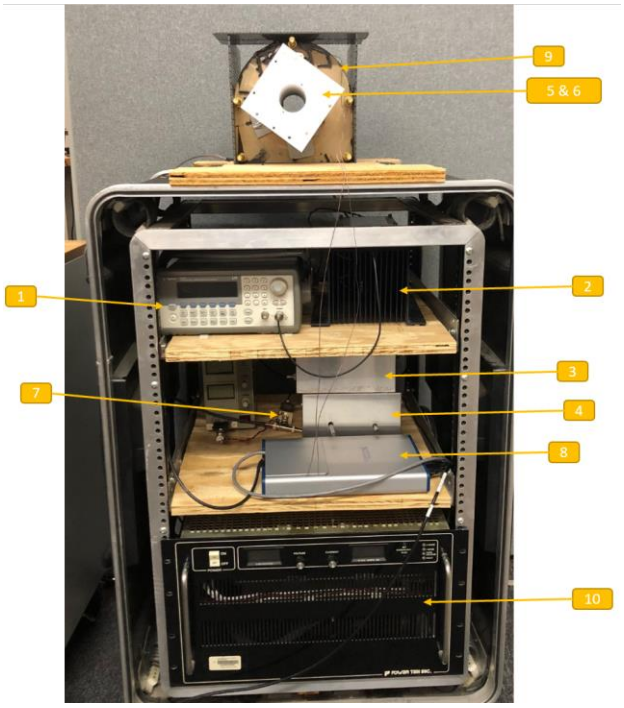

Figure 6. Picture of the MPI System. Each of the numbers are correlated with the numbers in Figure 5.

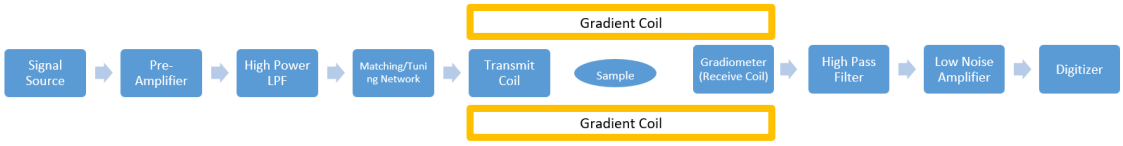

Figure 7. A block diagram of the main components of MPI.

Figure 6 is a picture of the final MPI system. An in-depth description of the MPI system will be discussed in Section II.6.

The following is a list of the hardware used in this project:

- Agilent 33220A Waveform Generator: a signal source that generates the 100 kHz fundamental frequency
- LZY-22+: a power amplifier from Mini circuits that amplifies frequencies from 100 kHz to 200 MHz and with a maximum output of 30 W

- Low-pass Filter: a high-power customized filter with a cutoff frequency at100 kHz to generate a pure signal at the fundamental frequency of 100 kHz
- Transmit Coil: a solenoid consisting of 131 windings, 12.05 cm length and a 6.8 cm diameter
- Receive Coil: a gradiometer placed coaxially in the center of the transmit coil made of 40 windings (2 cm length) and 45 tuning loops (2.5 cm length) and 4.2 cm in diameter.
- AU1647: a LNA by Miteq with a gain of 57 dB and a frequency range of 100kHz to 400 MHz for amplifying the signals and harmonics generated by the SPIONs
- NI USB-6353: 1.2 MS/s, 16-bit resolution used as an analog to digital converter (ADC).
- 25 nm SPIONs: manufactured by Ocean Nanotech with carboxylic acid side groups
- 20 nm SPIONs: manufactured by Nanocomposix

II.2 Transmit Chain Design

II.2.1 Transmit Coil Design Overview

The transmit coil needs to be slightly larger than the receive coil and smaller than the gradient coil. Using the size of a small rat as one of the design constraints, the transmit coil diameter needs to be at least 5 cm in diameters to contain the receive coil but smaller than 10 cm in diameter to fit within the brass tube. The transmit coil needed to be at least 10 cm long to allow the receive coil to have a tuning region. This will be

further discussed in Section II.2.4. Both the dimensions of the receive coil and gradient coil will be discussed in Sections II.3.2 and II.4.2, respectively.

II.2.2 Fundamental Frequency Signal Generation and Power Amplification Stage

The power delivered to the transmit coil is governed by the components of the transmit chain which consist of waveform generator, the power amplifier, the lowpass filter, and the matching/tuning network. The waveform generator provides the frequency content, the power amplifier amplifies the signal, the lowpass filter takes out any frequency above the excitation frequency, and the matching/tuning network transforms the transmit coil to the desired impedance, which our case is 50 Ω.

The fundamental frequency is generated by the Agilent 33220A waveform generator. The HP 54600B Oscilloscope will be used to measure the output of the waveform. Table 1 displays the output from the waveform generator.

Waveform Generator Voltage (Vpp)	Oscilloscope Measurement (Vpp)	Power (mW)	Power (dBm)
0.1	0.101	2.55×10^{-3}	-15.934
0.2	0.203	0.103	-9.871
0.3	0.301	0.227	-6.449
0.4	0.4	0.4	-3.979
0.5	0.5	0.625	-2.041
0.6	0.6	0.9	-0.458
0.7	0.7	12225	0.881
0.8	0.806	1.624	2.106
0.9	0.906	2.052	3.122
1	1.006	2.530	4.0313

Table 1. Oscilloscope measurement of the output from the waveform generator.

Power is calculated from the oscilloscope output. The relationship between the rms voltage and rms power for a sinusoidal waveform is described by the following equation:

$$P_{rms} = \frac{(V_{rms})^2}{R} \tag{12}$$

Where P_{rms} is rms power, R is resistance, and V_{rms} is rms voltage which is described by the following equation:

$$V_{rms} = \frac{\frac{V_{pp}}{2}}{\sqrt{2}} \tag{13}$$

The relationship between power (W) and power (dBm) is described by the following equation:

$$P_{dBm} = 10\log(\frac{P_W}{1\ mW}) \tag{14}$$

Where P_{dBm} is power in dBm and P_W is power in Watts.

Next, the gain after the power amplifier will be measured using the oscilloscope. Since the power amplifier produces a 30 W maximum output, a -30 dB attenuator will be used to protect the oscilloscope. Therefore, the values for the Oscilloscope Measurement (V_{pp}), Power (W), Power (dBm) will be attenuated by -30 dB.

Waveform Generator Voltage (Vpp)	Oscilloscope Measurement with -30 dB attenuator after power amplifier (Vpp)	Power after power amplifier with -30 dB (mW)	Power after power amplifier with -30 dB (W) (dBm)	Gain (dB)	Power after power amplifier (W)
0.1	0.575	0.827	-0.827	15.107	0.8266
0.2	1.144	3.272	5.1479	15.019	3.272
0.3	1.688	7.123	8.5268	14.976	7.123
0.4	2.25	12.656	11.023	15.002	12.656
0.5	2.797	19.558	12.913	14.954	19.558
0.6	3.312	27.423	14.381	14.839	27.423
0.7	3.844	36.941	15.675	14.794	36.941
0.8	4.344	47.176	16.737	14.631	47.176
0.9	4.75	56.406	17.513	14.391	56.406
1	5	62.5	17.959	13.927	62.5

Table 2. Oscilloscope measurement after power amplifier with -30 dB attenuator

Gain was determined by subtracting *Power (W)* in Table 1 from *Power after power amplifier with -30 dB* in Table 2. *Power after power amplifier (P)* was calculated using the following equation:

$$P = P_0 \times 10^{\frac{Gain}{10}} \quad (15)$$

Where P_0 is *Power (W)* from Table 1 and Gain is from Table 2.

Since the power amplifier can produce a max of 30 W before it starts producing spurious harmonics, 0.01 V_{pp} increments were measurements were taken after the 0.6 V_{pp} input signal as seen in Table 3.

Waveform Generator Voltage (Vpp)	Oscilloscope Measurement (Vpp)	Power (mW)	Power (dBm)
0.61	0.609	0.927	-0.328
0.62	0.615	0.946	-0.243
0.63	0.628	0.986	-0.061
0.64	0.634	1.00	0.0212
0.65	0.646	1.04	0.184

Table 3. Measurements taken after the waveform generator.

Waveform Generator Voltage (Vpp)	Oscilloscope Measurement with -30 dB attenuator after power amplifier (Vpp)	Power after power amplifier with -30 dB (W)	Power after power amplifier with -30 dB (W) (dBm)	Gain (dB)	Power amplified after power amplifier
0.61	3.344	0.0280	14.465	14.80	27.96
0.62	3.406	0.0290	14.624	14.87	29.00
0.63	3.469	0.0301	14.783	14.84	30.08
0.64	3.5	0.0306	14.861	14.84	30.63
0.65	3.594	0.0323	15.091	14.91	32.29

Table 4. Measurements taken after the power amplifier with -30 dB attenuator.

Therefore, upon closer inspection, 0.65 V_{pp} was chosen as the input waveform voltage, which provided approximately 32 W after the power amplifier and low pass filter stage.

II.2.3 Transmit Coil

The transmit coil provides the applied magnetic field on the SPIONs. It is critical to provide enough power to the transmit coil in order to drive the SPIONs into

saturation. There are two main factors that determine the excitation field generated transmit coil: the current delivered and the physical coil parameters. These two aspects will determine the magnetic field strength applied on the SPIONs.

The applied magnetic field experienced by the SPIONs will be approximated by three assumptions: (1) the particles are placed in the middle of the transmit coil, (2) the coil is much longer than the region of particles, and (3) the transmit coil has a homogenous field in the middle as illustrated in Figure 8.

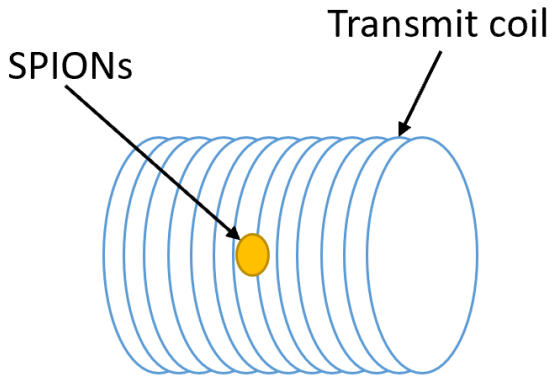

Figure 8. Illustration of transmit coil and SPIONs for Equation 16 showing that the particles are placed in the middle of the transmit coil and the coil being much longer than the region of particles.

Therefore, the equation for the applied external magnetic field, *H(t)*, can be generalized by the following equation [10]:

$$H(t) = \frac{N}{2\sqrt{\left(\frac{l}{2}\right)^2 + r^2}} i(t) \tag{16}$$

Where N is the number of loops, l is the length of the coil, r is the radius of the coil, and $i(t)$ is the current flowing through the coil. The current is derived from the

output power generated after the low pass filter stage. Assuming no loss in each stage of the transmit chain, the current is calculated by the following equation:

$$i(t)_{max} = \sqrt{\frac{P_{max}}{R}} \tag{17}$$

With P_{max} = 30 W and R = 50 Ω, $i(t)_{max}$ is approximately 0.77 A. The transmit coil had dimensions of 131 loops, a diameter of 6.8 cm, a length of 12.05 cm, and used AWG 22 wires. Therefore, the maximum applied magnetic field can be approximated using the following equation:

$$H(t) = \frac{131}{2\sqrt{\left(\frac{12.05\ cm}{2}\right)^2 + \left(\frac{6.8}{2}\ cm\right)^2}} i(t) \tag{18}$$

$$H(t) = 948.58 * 0.77 = 711.43 \frac{A}{m} * \frac{\frac{4\pi * 10^{-3} \frac{mT}{\mu_0}}{1\frac{A}{m}}}{} = 9.18 \frac{mT}{\mu_0} \tag{19}$$

Using the network analyzer, the transmit coil had an impedance of 3.15 + 146.912j Ω at 100 kHz as shown in Figure 9.

Figure 9. The network analyzer measured the impedance of the coil to be 3.15 + j146.9 Ω.

The capacitor values for the matching/tuning network was determined using the Smith V4.1 software program (https://www.fritz.dellsperger.net/smith.html). The matching capacitor needed to be approximately 8.1 nF and the tuning capacitor needed to be approximately 2.7 nF. The circuit diagram is shown in Figure 10.

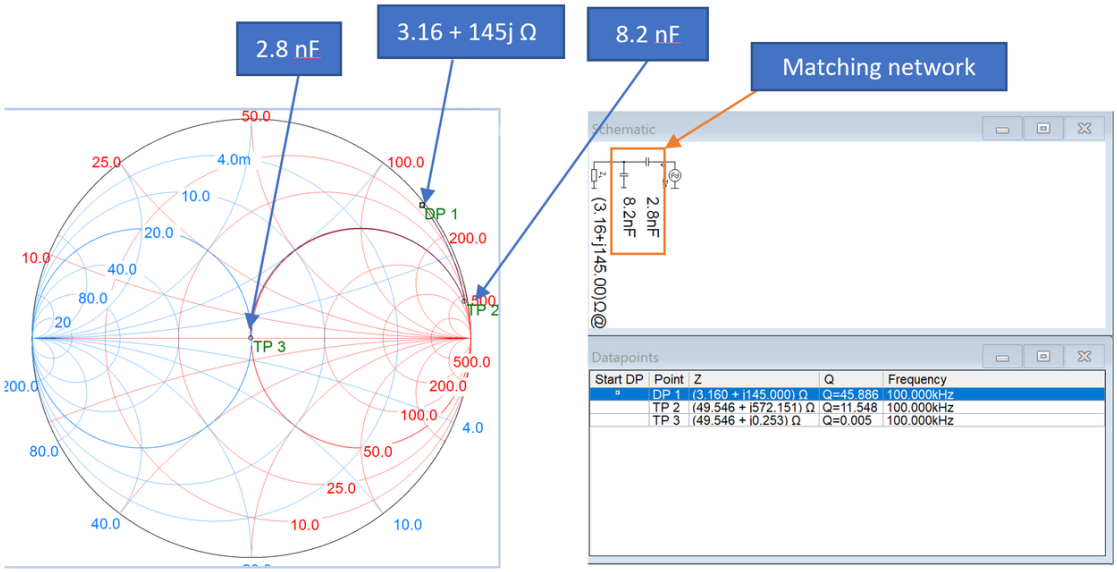

Figure 10. Smith v4.1 software program with matching and tuning network and Smith chart. The matching capacitor is approximately 8.2 nF and the tuning capacitor is approximately 2.8 nF.

The voltage rating required for the capacitors are critical in order prevent any of the components from breaking down. Multisim was used to find the necessary voltage ratings needed in the capacitors based on the circuit diagram provided from Smith 4.1v software.

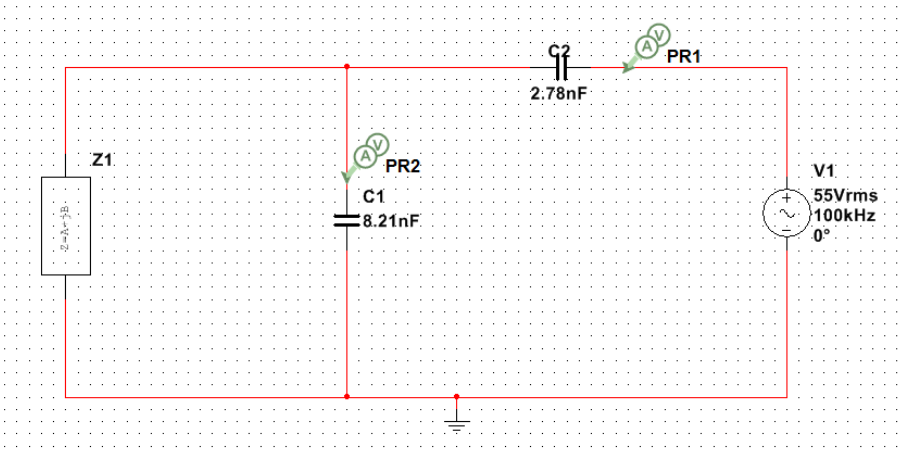

Figure 11. The circuit diagram to simulate the voltage & current experienced by the matching/tuning network in Multisim.

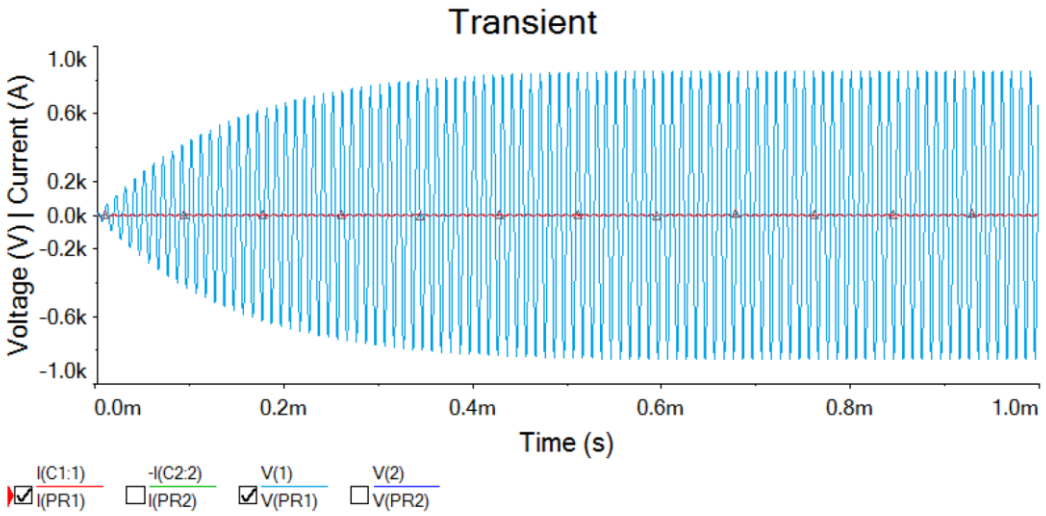

Figure 12. The voltage and current experienced by the matching capacitor (C1). The peak voltage at the matching capacitor is ± 1 kV.

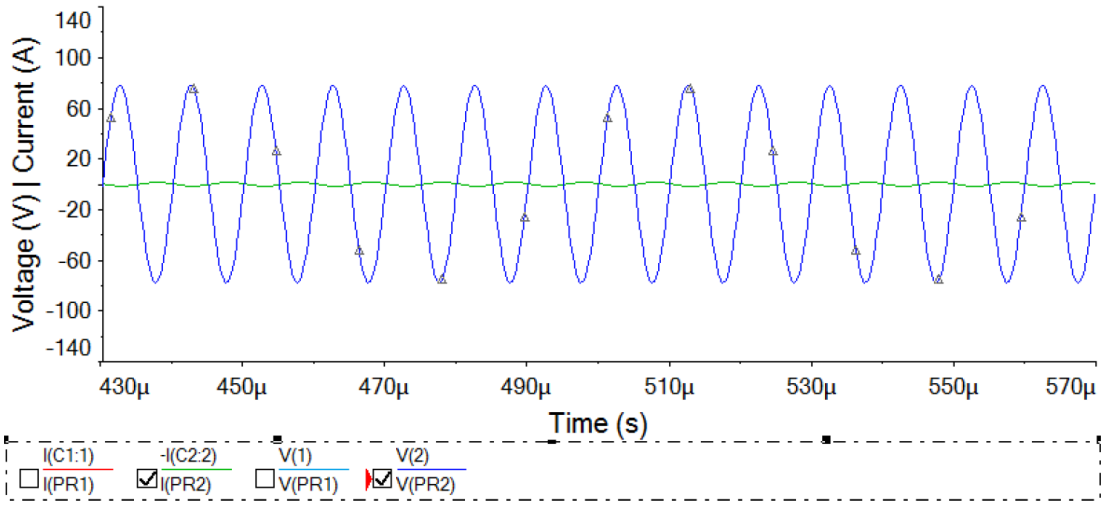

Figure 13. The voltage and current experienced by the tuning capacitor (C2). The voltage experienced at the tuning capacitor is approximately ± 80V.

The simulation indicated that the voltage and current that the voltage through capacitor 1 would peak at approximately 1kV and capacitor 2 would peak at approximately 80 V. In addition to purchasing capacitors that would meet those voltage ratings, two variable tuning capacitors (460 + 365 pF/1500 V) for the matching network and tuning network were used to get the precise capacitor values needed to match the transmit coil to 50 Ω.

The matching capacitor consisted of several 2200 pF capacitors as shown in Figure 14.

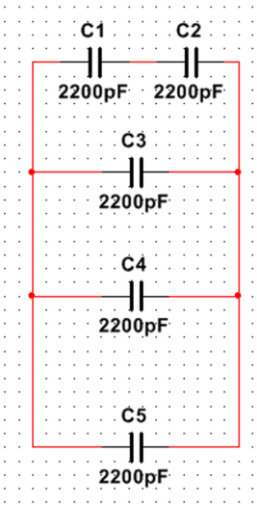

Figure 14. Capacitor values and circuit diagram for matching network.

The tuning capacitor consisted of two capacitors of 2000 pF and 270 pF as shown in Figure 15.

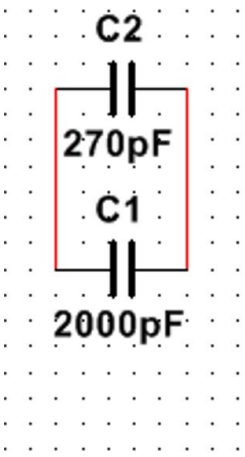

Figure 15. The capacitor values for the tuning network.

More information on the vendor, part number, and voltage ratings are available in Appendix A.

II.2.4 Transmit Coil Fixture Design

To fabricate the transmit coil, a transmit coil fixture must be designed first to provide structural support to the transmit coil. The transmit coil fixture was designed in SolidWorks. The first iteration of the transmit coil fixture is shown in the Figure 16. The transmit coil will be wrapped around the green portion in Figure 16.

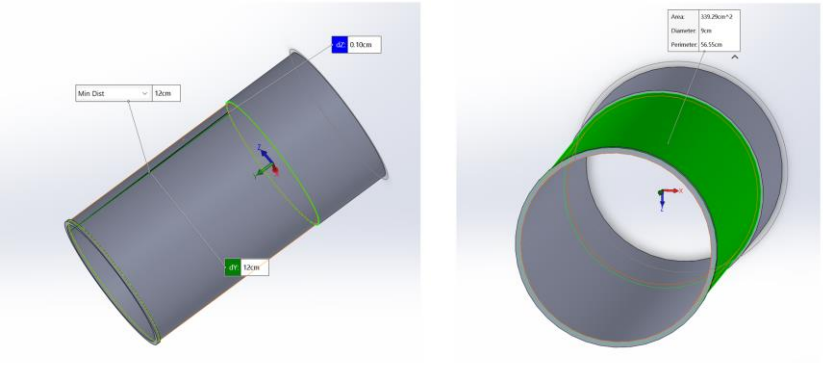

Figure 16. First iteration of transmit coil fixture. Only the diameter and length of the transmit coil were considered. The green region indicates where the wires will be wrapped.

The first design only considered the coil itself. However, in addition, the transmit coil fixture needed to consider how the transmit coil would be placed in reference to the gradient coil and how it would house the receive coil. It also did not consider how to the design would be fixed in respect to the receive coil and gradient coil. With these design considerations in place, three fixed support structures were placed along the coil to make sure that it would be fixed inside the gradient coil. The square end piece was also placed so that transmit coil fixture could be at a fixed in respect to the receive coil.

The final version of the transmit coil fixture is shown in Figure 17. The length of the transmit coil fixture was 12 cm and the circumference was 21.05 cm. The length and circumference provided a region enough for the receive coil to be placed inside.

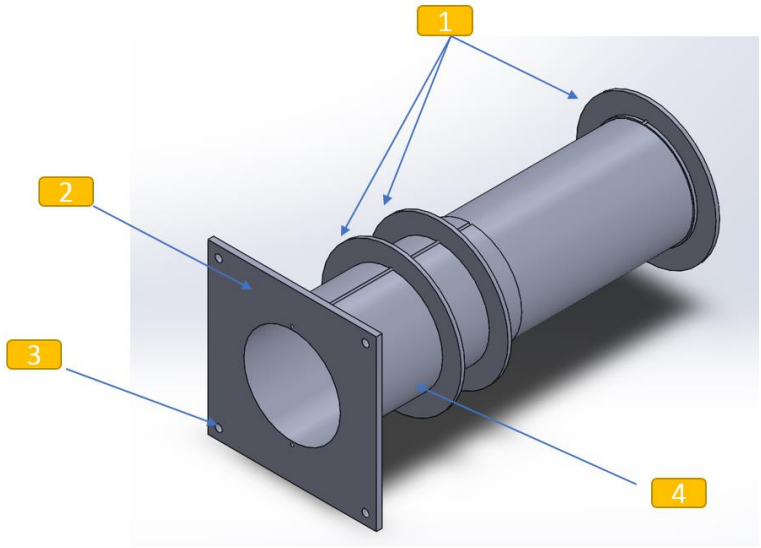

Figure 17. Final version of transmit coil fixture

The final version of the transmit coil fixture has several additional features:

(1) The support rings: three support rings were added to the design to make sure that the coil would have limited movement inside gradient coil.

(2) Square end piece: this ensured that the coil would be fixed in respect to the gradient and receive coil.

(3) Holes: these holes allow the transmit coil and receive coil to be fixed relative to each other.

(4) Additional space: the additional space was added to make sure there was sufficient length in the coil for the transmit coil to reach the null region in gradient coil.

The fixture was printed using PETG through 3dhubs.com.

II.2.5 Low Pass Filter Design

The low pass filter was used to filter out any frequencies above 100 kHz. After the power amplification stage, the power amplifier will create harmonics. If the harmonics are not removed, this will affect the signal of the receive coil. Therefore, having an input signal with only the fundamental frequency is critical.

The low pass filter is designed with a cutoff frequency of 100 kHz. The AADE Filter Design Tool (http://www.ke5fx.com/aadeflt.htm) was used to generate the capacitor and inductors needed to create the desired low pass filter. Figure 18 was generated by the design tool.

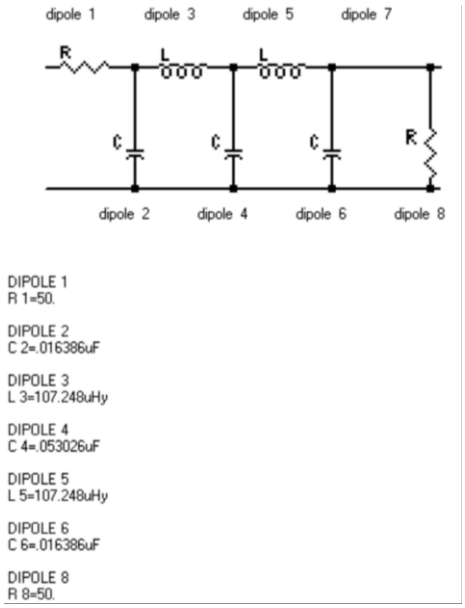

Figure 18. Low pass filter using the AADE Filter Design tool.

In order to create a high-power low pass filter, an inductor capable of handling high power needed to be custom made. Two inductors were created to be as close to 107

μH as possible as shown in Figure 18. Two inductors were created with 12 AWG wire with a diameter of 8.25 cm and length of 5.62 cm and a first layer of 25 turns and second layer of 13 turns. The inductor was approximately 106 μH.

Figure 19. Self-made high-power inductor for the low pass filter.

All the components (capacitors and inductors) were placed in an aluminum box. The inductors were placed perpendicular to each other to reduce the coupling between the inductors as seen in Figure 20.

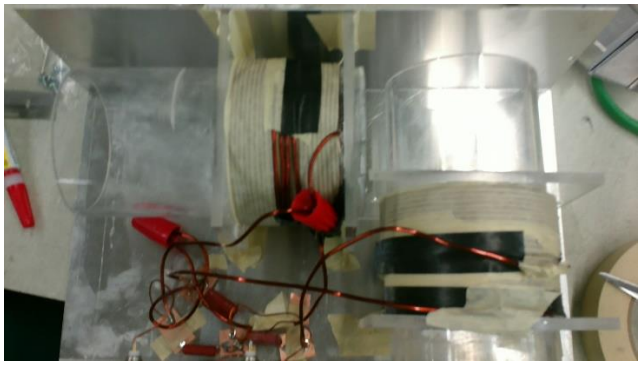

Figure 20. The internal components of the low pass filter. Notice that the inductors are orthogonal to each other to reduce coupling with each other.

The low pass filter had an attenuation of -1.36 dB at 100 kHz as shown in Figure 21, -22.28 dB at 200 kHz as shown in Figure 22, and -43.25 dB at 300 kHz as shown in Figure 23.

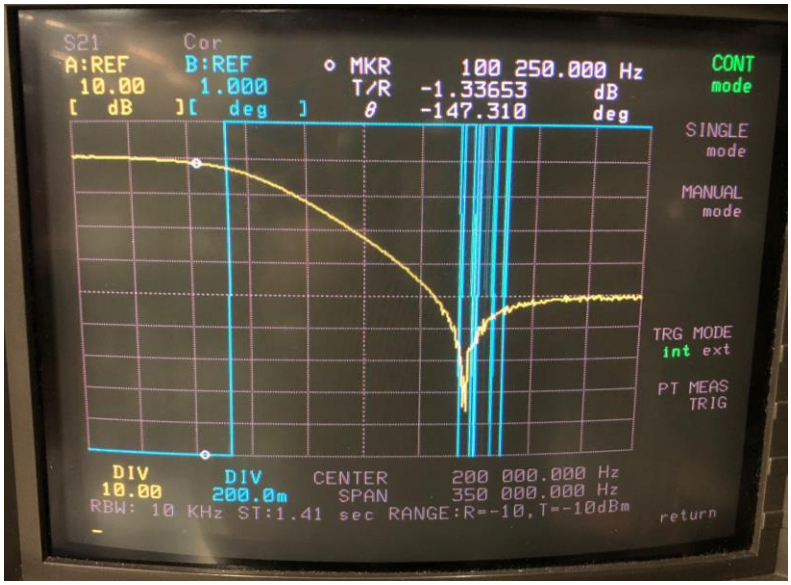

Figure 21. The S_{11} measurement shows a return loss at fundamental frequency is -1.34 dB.

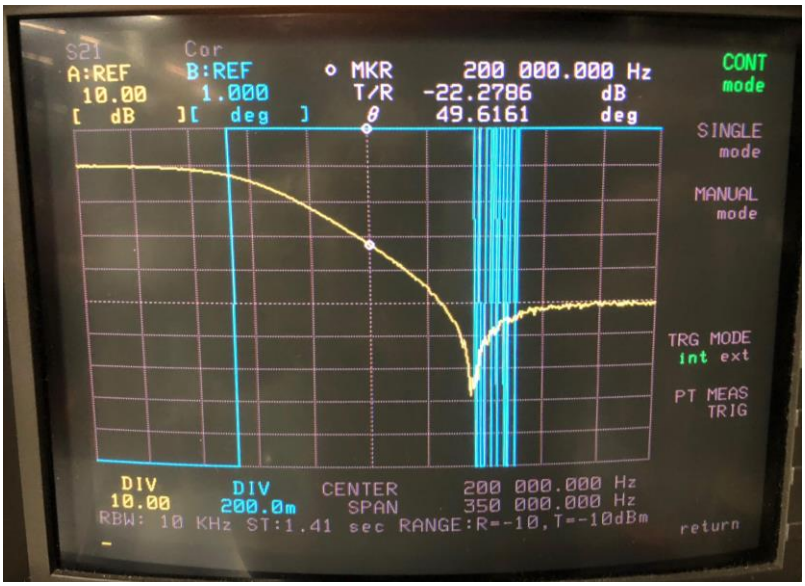

Figure 22. The S_{11} measurement shows a teturn loss at 2nd harmonic is -22.28 dB.

Figure 23. The S_{11} measurement shows a teturn loss at 3rd harmonic is -43.25 dB.

Waveform Generator Voltage (Vpp)	Oscilloscope Measurement (Vpp)	Power (W)	Power (dBm)	Gain	Power amplified after low pass filter
0.61	3.562	0.0317	15.013	15.341	31.720
0.62	3.625	0.0329	15.166	15.409	32.852
0.63	3.688	0.0340	15.315	15.377	34.003
0.64	3.750	0.0352	15.460	15.439	35.156
0.65	3.781	0.036	15.531	15.347	35.74

Table 5. Measurements taken after the low pass filter with the -30 dB attenuator

After accessing the performance of the low pass filter, 0.61 V_{pp} was chosen as the input voltage from the waveform generator. The output power after the low pass filter was 31.72; therefore, there was not much loss after the low pass filter stage. The current after the low pass filter is still approximately 0.75 A and the applied magnetic field is still approximately $9.18\frac{mT}{\mu_0}$.

A side note on the low pass filter: The lid of the low pass filter had to be isolated from the box. When the lid touched the box, the performance of the low pass filter significantly became worse as seen in Figure 24, Figure 25, and Figure 26. The return loss for the fundamental frequency was -13.26. The return loss for the 2nd harmonic was -17.55 dB. The return loss for the 3rd harmonic was -25.47 dB.

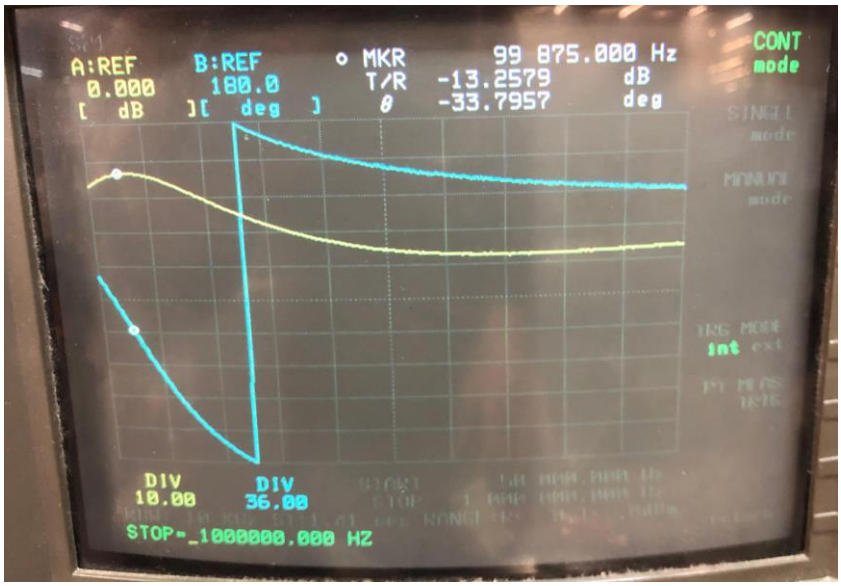

Figure 24. Return loss of the fundamental frequency was -13.26 dB when the lid is touching the box.

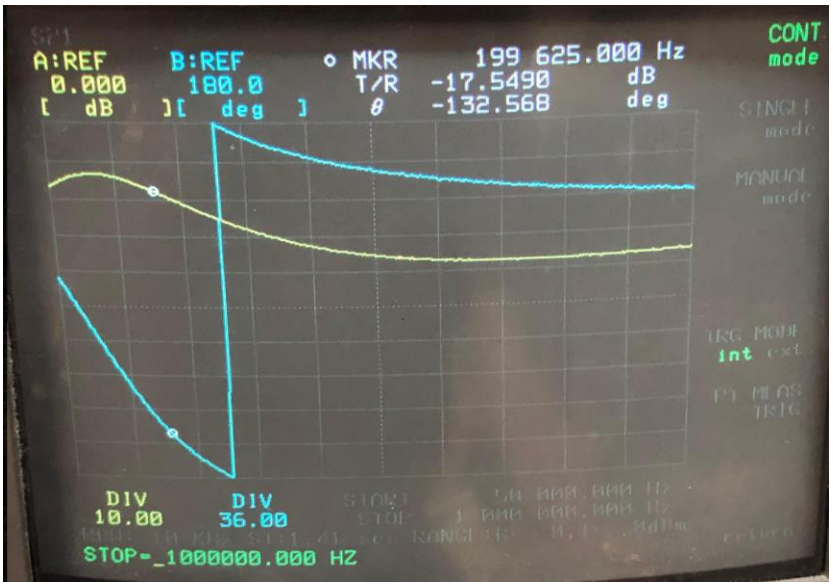

Figure 25. Return loss of the 2nd harmonic was -17.55 dB when the lid is touching the box.

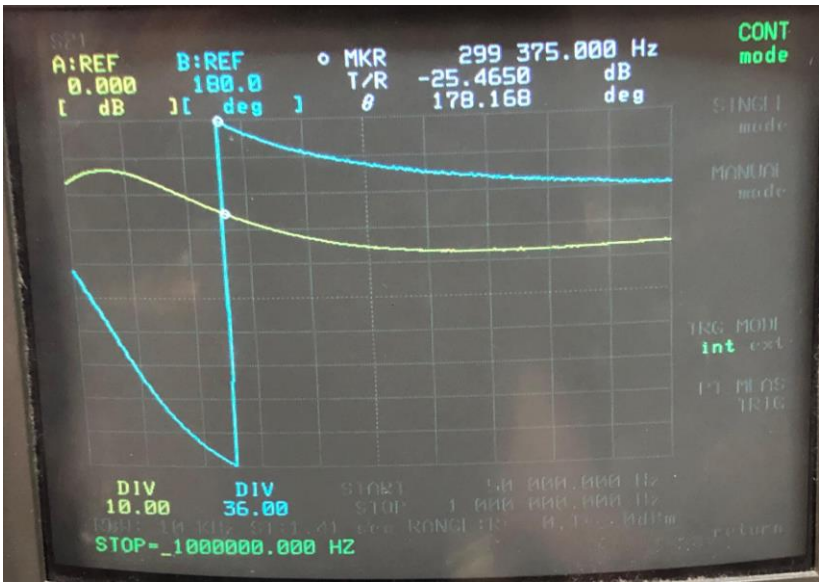

Figure 26. Return loss of the 3rd harmonic was -25.47 dB when the lid is touching the box.

When current was flowing through the low pass filter, there was probably mutual inductance occurring between the inductors of the low pass filter and the box.

II.3 Receive Chain Design

II.3.1 Receive Coil Design Overview

The purpose of the receive coil is to pick up the change in magnetization from the SPIONs. Therefore, the diameter of the receive coil needs to be at least 3 cm for a small mouse/rat sized-phantom. The length of the receive coil needs to be at least the same dimension as the resolution of the system. However, the signal improves with more loops and length. For our system, since size is a major consideration, the length of the signal pickup loop region was limited to 2 cm which is slightly less than the separation distance between the two coils for the gradient coil.

II.3.2 Receive Coil Design

The receive coil is a pickup loop to detect SPION magnetization change. Based on the law of induction, a change in magnetization will change the voltage induced across a solenoid. Since the receive coil picks up the fundamental frequency generated by the transmit coil, in addition to the loops that will pick up the signal, a tuning loop will be used to cancel out the fundamental frequency generated by the transmit coil. This type of coil configuration is also known as a gradiometer [14].

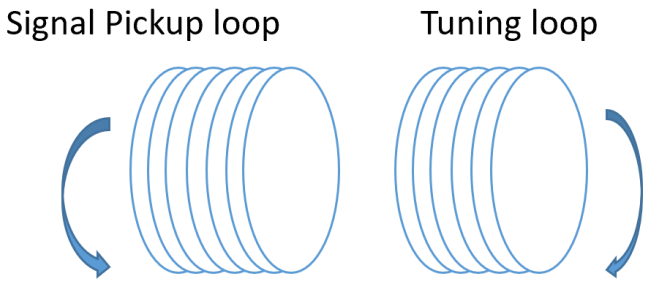

Figure 27. A representation of a gradiometer. The gradiometer consists of two main portion: the signal pickup loop and the tuning loop.

Therefore, the gradiometer will consist of two solenoids in series, but the solenoids will be in opposite direction. When the particles are placed in the signal pickup loop, the signal from the receive coil will be from the SPION magnetization response. The signal pickup portion of the gradiometer had 40 loops, a radius of 2.35 cm, length of 2 cm while the tuning loops of the gradiometer will have 45 loops, a radius of 2.35 cm, and length of 2.3 cm. The signal pickup loops and the tuning loops will be spaced by 3 cm.

In retrospect, the signal pickup portion of the gradiometer should have had more loops and longer length. With more loops and longer length, the gradiometer will pick up more of the of SPION magnetization changes. However, the initial receive coil design was going to be a saddle coil which will be discussed further in Section II.3.5.

While the transmit coil had a filter to exclude all frequencies beside the fundamental frequency, the receive coil chain did not utilize a filter. For the transmit coil, the signal coming in needs to be at the fundamental frequency. However, for the receive coil chain, in addition to the fundamental frequency, we are interested in the harmonics. Therefore, a filter was not implemented after receive coil.

II.3.3 Receive Coil Fixture Design

The receive coil fixture was used to house the gradiometer coil and has a similar design to the transmit coil fixture. The receive coil fixture was modeled in SolidWorks and shown in Figure 28.

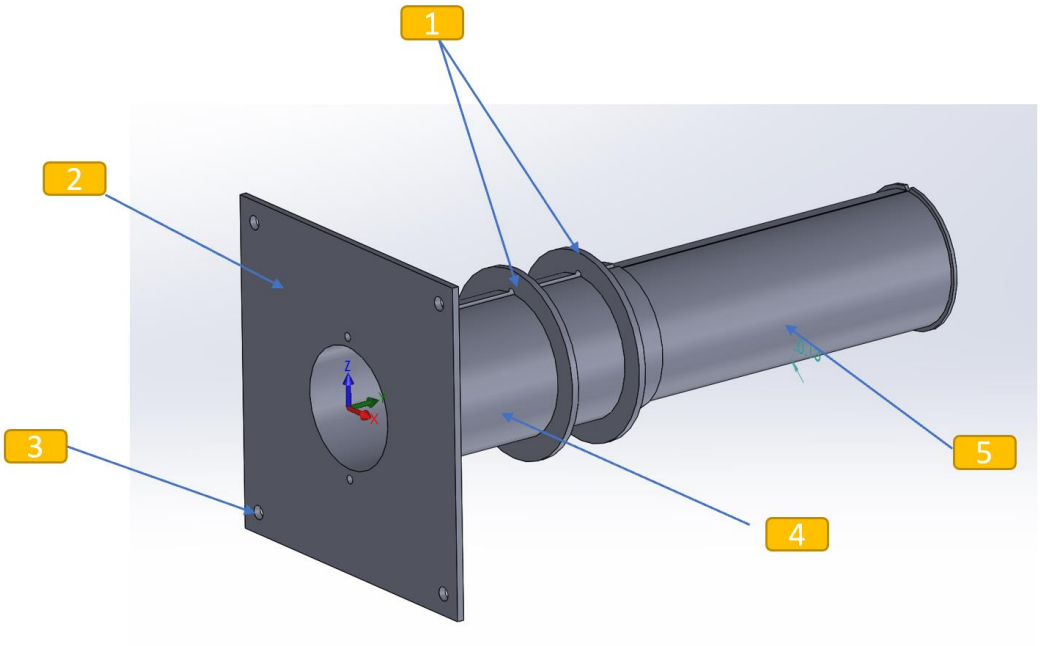

Figure 28. Final design for the teceive coil fixture.

The gradiometer had a few additional features:

(1) Support rings: two support rings were added to the design to make sure that the coil would not move around inside transmit coil.

(2) Square end piece: this ensured that the coil would be at a fixed length in respect to the receive coil.

(3) Holes: these holes allow the transmit coil and receive coil to be fixed relative to each other

(4) Additional space: the additional space was added to make sure there was sufficient length in the coil for the receive coil to reach the null region in gradient coil.

(5) Gradiometer portion: this is where the gradiometer would be wrapped around the fixture. The length of the portion was 12 cm and the radius was 2.35 cm.

The fixture was printed using PETG through 3dhubs.com.

II.3.4 Receive Chain

The other components of the receive chain consisted of the LNA AU1647 and the NI USB 6353. The LNA is used to amplify the magnetization signals generated by the SPIONs and the NI USB 6353 was used to collect the data.

II.3.5 Notes on Receive Coil Options

There were a couple of receive coil options that were taken into consideration. One was the gradiometer; the other was a saddle coil. The saddle coil has an advantage over the gradiometer in that the loops are orthogonal to the direction of the applied magnetic field. However, since they sit orthogonal to the applied magnetic field, they will also detect less of the change in magnetization of the SPIONs.

Another disadvantage of the saddle coil was its fabrication process. First to create an appropriate fixture for the saddle coil proved to be challenging. Since the saddle coil had a saddle shape, wrapping wires around a saddle shaped fixture was very difficult. Bending the wires 90 degrees and staying close to the saddle fixture was difficult as well. Since the fabrication process was difficult, the decoupling between the saddle coil as the receive coil and the transmit coil was not better than the gradiometer. Therefore, the gradiometer design was chosen over as the saddle coil as the receive coil.

II.4 Gradient Coil Design

II.4.1 Gradient Coil Design Overview

In MPI, gradients govern the resolution of the system, provide spatial information, and determine the speed of the MPI system. The purpose of the gradient is to provide a field free region (FFR) while providing a magnetic field that would saturate the magnetization of the particles outside of the FFR. For this project, only one gradient set was used, therefore, the gradient produced a field free plane (FFP). The gradient set were designed using coils. Some major considerations for designing gradient coils were the wire size, wire shape, the fusing current of the wire, coil size, coil radius, and the current.

As mentioned previously in the project aims (Section I.8), the goal is to achieve clinical relevance for imaging. SPIONs eventually accumulate in the liver after injection [17]. With the size of rat's liver around 20 mm in length, the target resolution produced by the gradient set will need to reach at least 2 mm resolution to provide a 10-pixel resolution across the object. Using a particle size of 25 nm, the gradient strength will need to be at least 2 mT/mm. The gradient set will be a set of two coils constructed using magnet wire. However, additional design considerations were needed and were addressed in the design options below:

Design 1: The first design consideration was to use an electromagnet as the gradient coil. The electromagnet will require a high current power supply to generate a strong gradient field. In addition, since there will be high current flowing through the

electromagnet, the power supply will need to run at a low duty cycle to prevent the gradient from overheating and fusing.

Design 2: A gradient can also be produced by using two permanent magnets. Two ring magnets can be placed with the polarities facing towards each other, which will produce a gradient. The main advantage for this approach is that there is no need of a gradient amplifier, which will significantly decrease the weight of the MPI system. However, the mechanical structure involved in fixing the magnets will need to be extremely stable and strong. In addition, this design could potentially be a safety hazard since it involves two permanent magnets.

Both designs come with engineering obstacles. Design 1 requires a high current power supply. Typically, the stronger the power supply the larger the power supply. This is contrary to the goal of designing for a portable system. For Design 2, the mechanical fixture needs to be able to constantly keep the permanent magnets in place. However, for this project, the main consideration was safety. Design 1 allows the user to turn off the gradient field when the system is not in use, while Design 2 is a permanent magnet which makes it a continuous safety hazard.

Another critical aspect of designing the gradient is moving the FFP across the object. There are two approaches in moving the FFP in MPI: mechanical or electrical motion. Both approaches have their own advantages and disadvantages. Three options were considered:

Option 1: Mechanical movement of the object being imaged. In this approach, the object will move incrementally across the FFP. For this approach the main advantage

is that there will be no need of increasing the current or including a bias coil to move the FFP around. The main disadvantage is that with mechanical movement of the object, this limits the speed of the imaging process.

Option 2: Mechanical movement of the gradient coil. In this approach, the gradient coil will move across the object. This will keep the object stationary in respect to the FFP. Again, the main advantage of this approach is that there is no need of increasing the current of the gradient coil or including a bias coil to move the FFP around. However, similar to option 1, the mechanical movement of the gradient coil will limit the speed of the imaging process.

Option 3: Electronic movement of the FFP. In this approach, both the gradient coil and the object will be stationary. To move the FFP, there are potential two methods: one is to increase the current through the gradient coil and the other is to include a bias coil that will move the FFP. For the first method, the FFP will move when the current through one gradient coil increases while the other gradient coil stays the same. This will allow the FFP to move across the region of interest. Method 2 is to introduce a bias coil. The bias coil will be a separate pair of coils powered by a separate current supply. The bias coil will be responsible for moving the FFP across the object. The main advantage of this option is there will be no moving parts and a faster imaging speed. However, the disadvantages are that a much higher current will be needed to move the FFP around and as the FFP move to the edge of the region of interest, the speed and resolution will change.

Option 1 was chosen for this MPI system. Option 1 provides the best outcome for the desired resolution, keeping the system portable and the design simple. With option 2, when the gradient coil moves, that will change the matching/tuning of the transmit and receive, in addition to the inductance experienced by the system coils. Option 3 is difficult because to image an entire rat/mouse, the separation distance between the gradient coils needs to be at the very least the length of the animal. Therefore, with a larger coil separation distance, the current needs to be greater to maintain a high gradient. Therefore, option 1 is the best solution since the gradient coils can be placed closer together to create a stronger gradient field and then the object can move through the FFP.

To sum up the design considerations, the gradient will be an electromagnet and the object will move through the FFP of the gradient coil.

II.4.2 Gradient Coil Simulation

MATLAB was used to find the most optimal parameters with a target of 2 T/m. The MATLAB program, Gradient_Coil_Optimization_Approx_RevB.m, can be found in Appendix B**Error! Reference source not found.**. The MATLAB program optimizes the parameters for the gradient by the user. Several physical parameters of the gradient coil were defined with size and portability being the priority. Therefore, the desired gradient strength, the coil width, the coil length, coil separation, and the radius of the coil were pre-determined by the user. After determining these parameters, the current per loop (*IN*), the number of loops per layer (*N*), and the total number of layers (*layers*) were extracted from the defined parameters. Then the program finds the magnetic field

contribution from each layer, the gradient strength, the current, the resistance, the power and the voltage for a range of wire diameters. When using the program, the desired gradient strength should be higher than the intended gradient strength. When the program is optimizing the optimal number of layers, it chooses an integer number of layers closest to the desired gradient strength. For example, if the desired gradient strength is 2.5 T/m, a hypothetical output for 10 layers could be 2 T/m and a hypothetical output for 11 layers could be 3.5 T/m. The program will choose 10 layers for the simulation since 2 T/m is closer to 2.5T/m than 3.5 T/m. Figure 29 and Figure 30 are the results of the simulation. As we can see the gradient strength and magnetic field does not change as the wire diameter changes. This is interesting but somewhat expected since the coil length, width, radius, and separation distance are all fixed, that means the current density is going to be constant. Therefore, the gradient strength and magnetic field is going to be very similar for the range of wire diameter. The resistance drastically increases as wire diameter decreases.

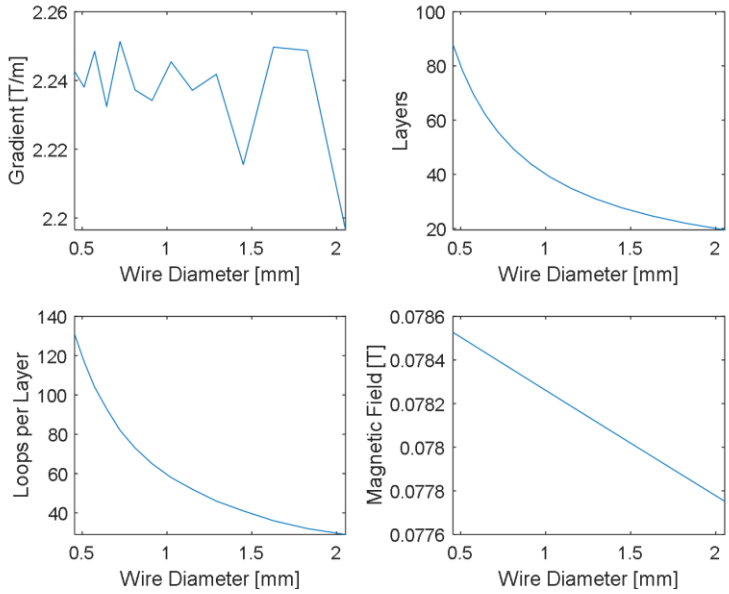

Figure 29. The gradient strength ranged from 2.2 to 2.25 for range of wire diameters (Top-Right). The layers needed for the target gradient strength as a function of wire diameter (Top-Left). The loops per layer needed to reach the gradient strength shown in the top-right graph (Bottom-Left). The magnetic field generated from each gradient coil as a function of wire diameter (Bottom-Right) Defined Parameters: Inner Radius - 6 cm, Target Gradient Strength - 3 T/m, Coil Separation - 4 cm, Coil Width - 4 cm, Coil Length - 6 cm

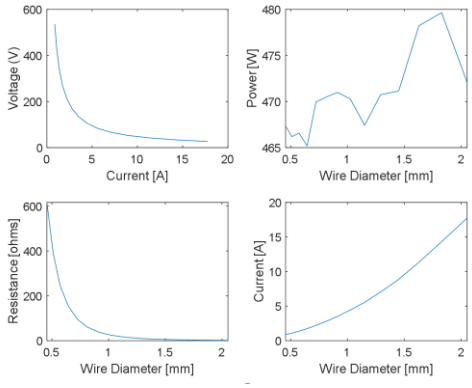

Figure 30. The voltage needed to generate the gradient strength as a function of current (Top-Right). The power required for a power amplifier in order to generate the desired magnetic field (Top -Left). The resistance of the gradient as a function of the wire diameter used to fabricate the gradient coil (Bottom – Left). The current needed to generate the gradient with the associated wire diameter used to fabricate the gradient coil (Bottom – Right). Defined Parameters: Inner Radius - 6 cm, Target Gradient Strength - 3 T/m, Coil Separation - 4 cm, Coil Width - 4 cm, Coil Length - 6 cm

AWG	wire_diameter	gradient	B_field	power	resistance	Current
12	0.002053	2.1965	0.077752	472.04	1.499	17.746
13	0.001828	2.2487	0.07786	479.65	2.3392	14.319
14	0.001628	2.2497	0.077957	478.22	3.7215	11.336
15	0.00145	2.2155	0.078043	471.14	5.9949	8.8651
16	0.001291	2.2418	0.07812	470.73	9.5112	7.0351
17	0.00115	2.2371	0.078188	467.42	15.21	5.5436
18	0.001024	2.2454	0.078249	470.28	24.011	4.4256
19	0.000912	2.2342	0.078304	470.99	38.076	3.5171
20	0.000812	2.2372	0.078352	470.48	60.516	2.7883
21	0.000723	2.2514	0.078396	469.96	96.208	2.2102
22	0.000644	2.2324	0.078434	465.19	154.39	1.7358
23	0.000573	2.2485	0.078469	466.57	244.61	1.3811
24	0.000511	2.2381	0.078499	466.19	388.95	1.0948
25	0.000455	2.2427	0.078527	467.34	616.52	0.87064

Table 6. Summary of the plots in Figure 29 and Figure 30.

AWG	wire_diameter	layers	N	Total_Loops
12	0.002053	19.484	29	565.03
13	0.001828	21.882	32	700.22
14	0.001628	24.57	36	884.52
15	0.00145	27.586	41	1131
16	0.001291	30.984	46	1425.3
17	0.00115	34.783	52	1808.7
18	0.001024	39.063	58	2265.6
19	0.000912	43.86	65	2850.9
20	0.000812	49.261	73	3596.1
21	0.000723	55.325	82	4536.7
22	0.000644	62.112	93	5776.4
23	0.000573	69.808	104	7260
24	0.000511	78.278	117	9158.5
25	0.000455	87.912	131	11516

Table 7. Continuation of the summary of the plots in Figure 29 and Figure 30.

Since the gradient strength does not change much with the wire diameter used for fabrication, main consideration for wire diameter is the fabrication difficulty and finding a gradient power amplifier with the appropriate physical and electrical specifications. Most power amplifier that use a standard electrical outlet can generate around 10 A. This limits the wire choices to AWG 15 and higher. In addition, portable power amplifiers with a 10 A rating will have approximately a voltage rating of 120 V. This limits the wire choices to AWG 19 and lower. Therefore, based on these considerations, AWG 17 was chosen as the wire size to fabricate the gradient coil.

Another program, Gradient_Coil_Calculations_v2.m (Appendix C**Error! Reference source not found.**), was developed to simulate the gradient strength while changing the current (*Current*), the number of loops (*N*), and layers (*layers*). In addition, the way the magnetic field was simulated is slightly different from the previous program. While the previous program used an approximation to determine the magnetic field, this program analyzed the contribution magnetic field of each loop. As seen in Figure 31, a gradient strength of 2 T/m is produced from using AWG 17 wire with 20 layers, 50 turns per layer, a coil separation distance of 4 cm, and 11 A of current.

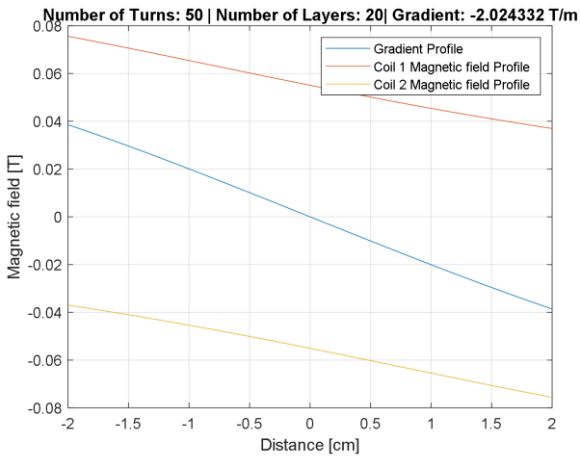

Figure 31. The gradient strength produced by the defined parameters was 2.02 T/m. Each individual coil needs to produce 0.08 T to create the desired gradient strength. Parameters: wire diameter - 1.22 mm, inner radius – 5.78, coil separation – 4 cm, number of loops – 50, number of layers – 20, and current – 11 A.

II.4.3 Gradient Coil Fabrication

The gradient coil was fabricated based on the simulation parameters stated in Section II.4.2 (AWG 17, inner radius of 5.78 cm, coil separation of 4 cm, 50 loops per layer, 20 layers, and 11 A of current). The gradient coil was wrapped around a thick brass tube. In addition to acting like a fixture for the gradient coil, the brass tube also

was used as a shield for the transmit coil and receive coil to block any potential noise sources. For example, the brass tube acts as a passive shield to reduce the non-linearities produced by the gradient, which would produce harmonics picked up by the receive coil [16]. The brass tube has a length of 33 cm and outer radius of 11.43 cm and inner radius of 10 cm.

A coil winding jig was built to transfer the spool of wire to the brass tube. The coil winding jig is shown in Figure 32.

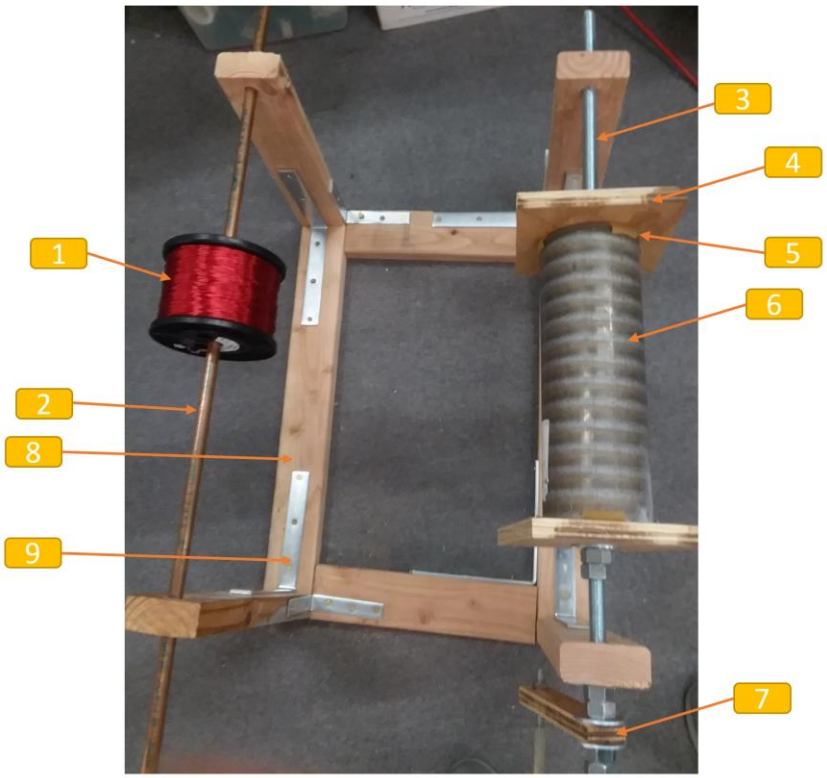

Figure 32. Coil Winding Jig

(1) The spool of AWG 17 wire that needs to be transferred to the brass tube

(2) A rod is used to hold the AWG 17 wire

(3) The sturdy rod is used to hold the brass tube. This rod needs to be able to handle the weight of the brass tube in addition to the wire transferred to the brass tube.

(4) The wooden place holds the brass tube in place.

(5) The rubber material prevents the brass tube from slipping

(6) The brass tube is where the wire will be transferred to.

(7) The handle and lever helped rotate and transfer the wire to the brass tube.

(8) The jig consists of eight wooden pieces.

(9) The metal L brackets were used hold the wooden pieces in place.

In addition, side pieces were included to keep the wires in place and mark the location of the gradient coil as seen in Figure 33. Even though the coil winding jig helped transfer the spool of wire to the brass tube, the process was still extremely difficult. As seen from Figure 33, the layers and wires are difficult to observe since all the layers were red. In addition, since the wires are cylindrical, the wires may not line up in place. For the first layer this is not a problem. All the wires line up well and are on the same layer. However, as the layers progress, it becomes increasingly difficult to keep all the wires perfectly close together. As a result, this problem cascades for each successive layer.

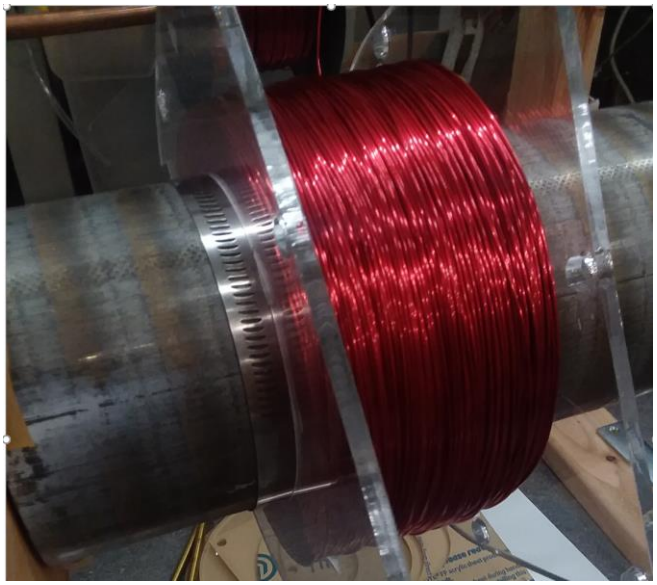

Figure 33. A picture of the side pieces using the metal tube clamps to fix them in place while the gradient coil (red wire) is being wrapped around the tube.

Gradient coil fabrication is a challenging feat. In a later section, there will be more discussion on potential solutions to improve the design in the future.

II.5 SPIONS

II.5.1 SPION particles

25 nm and 30 nm SPIONs were purchased from Ocean Nanotech. The particles came in 1 mL with 5 mg/mL concentration.

II.5.2 SPION Particle Concentration

One of the advantages of MPI is its potential for high sensitivity. In a 2017 paper on MPI, a sensitivity limit was reported at 200 nM [12]. The molecular formula for SPIONs is Fe_2O_3 and the molecular weight is 159.69 g/mol [16]. The following equation converts SPIONs from molar to mg/mL.

$$Molar\ Concentration\ \left[\frac{mol}{ml}\right] \div Molecular\ Weight\ \left[\frac{mg}{mol}\right] = Density\ \left[\frac{mg}{ml}\right] \quad (20)$$

$$200 \times 10^{-9} \frac{mol*Fe}{L} \times \frac{1\ L}{1000\ ml} \times \frac{1\ Fe_2O_3\ particle}{2\ Fe\ particles} \times 159.69 \frac{g}{mol} \times \frac{1000\ mg}{1\ g} \quad (21)$$

$$= 1.6 \times 10^{-5} \frac{mg}{mL}$$

The following equation converts density to particles/mm^3:

$$Density\ \left[\frac{g}{L}\right] \times \frac{1\ L}{10^6\ mm^3} \times \frac{1\ Fe_2O_3\ particle}{4.287^{-14} g} = \ Concentration\ \left[\frac{particles}{mm^3}\right] \quad (22)$$

Therefore, the density of $200 \frac{nmol*Fe}{L}$ is approximately 372.5 $\frac{particles}{mm^3}$. While our MPI system will not reach this target, we will aim for two orders of magnitude higher which will be approximately 4×10^4 $\frac{particles}{mm^3}$.

II.6 MPI System

The final MPI system setup is shown in Figure 34.

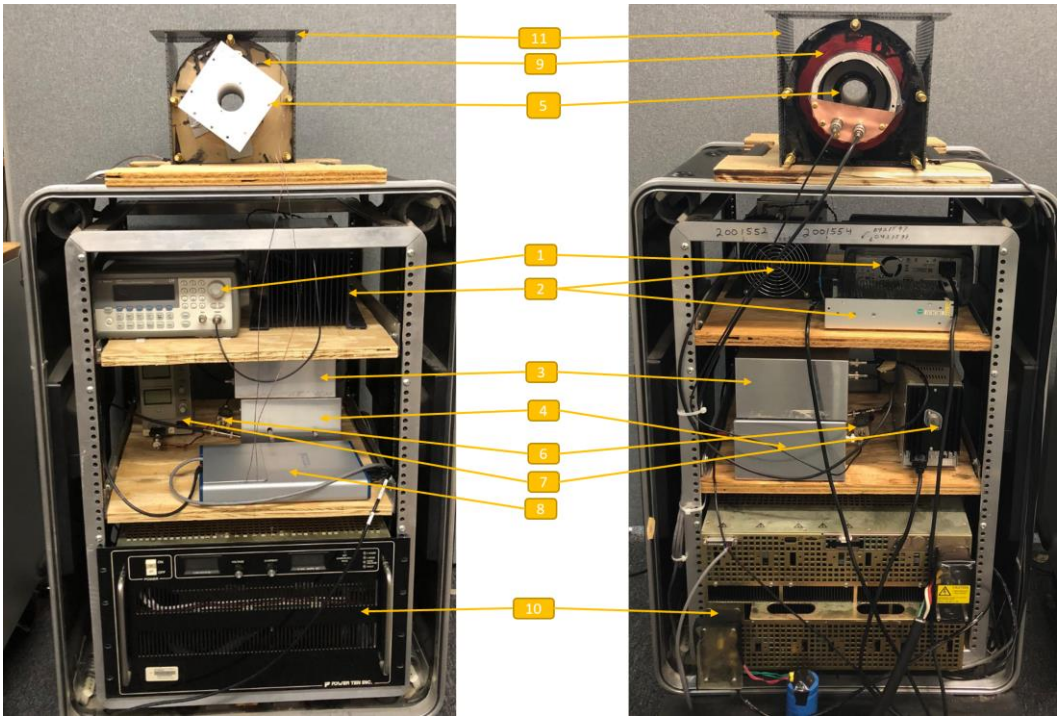

Figure 34. (Left) Front side of the MPI system. (Right) Back side of the MPI system.

(1) Waveform generator: Provides the excitation frequency for the MPI system.

(2) Power amplifier: Amplifies the signal coming from the waveform generator.

(3) Low pass filter: Filters frequency content lower than 100 kHz.

(4) Matching/tuning network: Converts the impedance of the transmit coil to 50 Ω.

(5) Transmit coil and receive coil: generates the excitation field (transmit coil) and picks up the signal from the SPIONs (receive coil). The transmit coil and receive coil are contained inside the white 3D printed object.

(6) Low noise amplifier (LNA): Amplifies the signal picked up by the receive coil.

(7) DC power supply: Powers the LNA.

(8) DAQ: Acquires the data from the LNA.

(9) Gradient coil: Generates the selection field

(10) Gradient power supply: Provides the current to generate the selection field in the gradient coil.

(11) Plastic casing: Provides protection for the gradient coil. The casing is perforated to promote cooling for the gradient coil.

II.7 LabVIEW

LabVIEW 2017 (64-bit) was used to develop the software to control the gradients and perform data acquisition. The NI USB 6353 DAQ was used as the data acquisition unit to capture the signal.

II.7.1 LabVIEW Block Diagram

The LabVIEW block diagram (Signal Analysis.vi) is responsible for controlling the DAQ to collect the measurements from the receive coil, process the data, and monitor temperature. Figure 35 shows the block diagram.

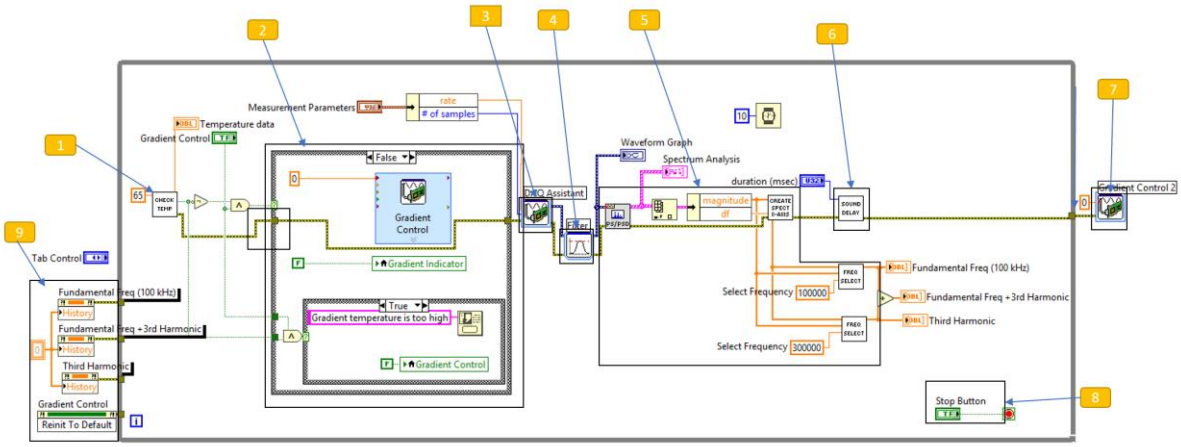

Figure 35. LabVIEW Block Diagram

(1) Checks the temperature. If the temperature is higher than the designated peak temperature, then the DAQ will turn off the gradient. The CHECK TEMP subVI (temperature check.vi) is shown in Figure 36.

(2) Controls the gradients based on the output of the CHECK TEMP subVI and the gradient control indicator.

(3) Makes a measurement based on the specified rate and # of samples.

(4) Digital high pass filter at 70 kHz.

(5) This section converts the time domain signal into the frequency domain. The CREATE SPECT X-AXIS subVI (Create Frequency Axis.vi) extracts the information for x-axis for the spectral domain. The block diagram and front panel is shown in Figure 37. The

FREQ SELECT subVI (Frequency selection.vi) returns the value of the selected frequency and is shown in Figure 38.

(6) The SOUND DELAY subVI (Delay sound.vi) creates a sound delay that gives the user time to move the sample. This will eventually be replaced with a VI that moves the sample using a stepper motor. The front panel and block diagram are shown in Figure 39.

(7) Turns off the gradient.

(8) Stops the program.

(9) Reinitialize all the graphs and gradient control to their default values.

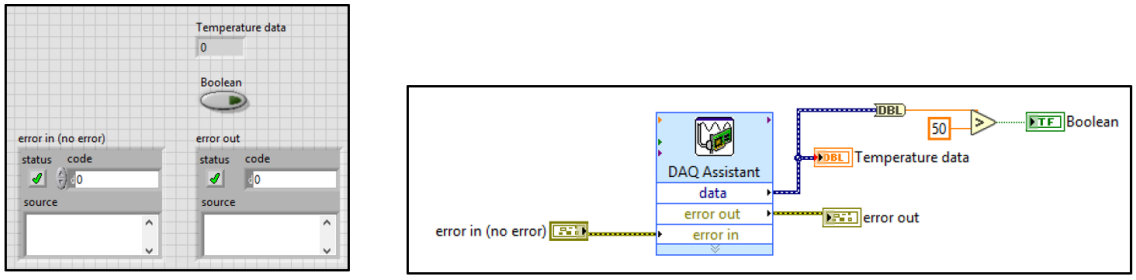

Figure 36. Check Temp subVI. (Left) Front Panel (Right) Block Diagram

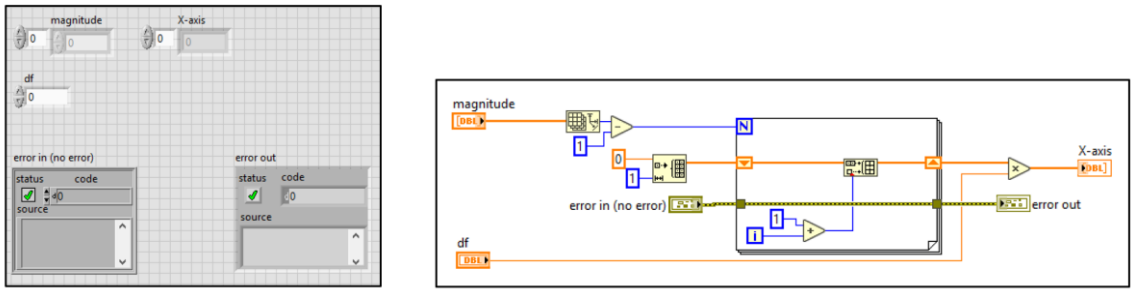

Figure 37. Create Frequency Axis subVI. (Left) Front panel (Right) Block Diagram

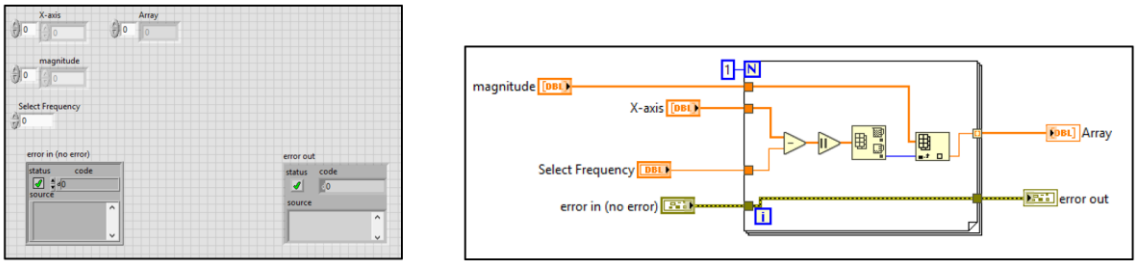

Figure 38. Frequency Selection subVI. (Left) Front panel (Right) Block Diagram (Left)

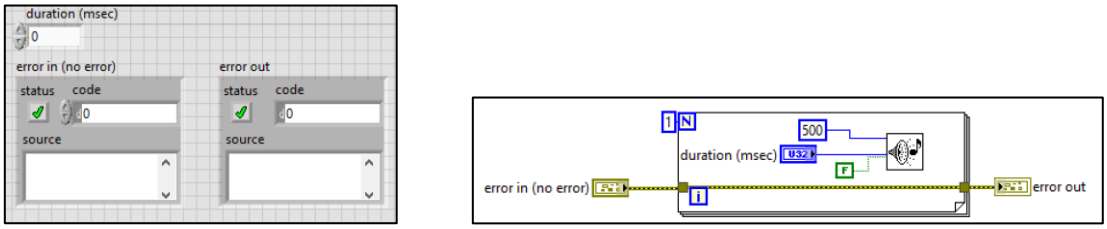

Figure 39. Delay Sound subVI. Front panel (Right) Block Diagram (Left)

II.1.1 LabVIEW Front Panel

The LabVIEW front panel is shown in Figure 40. The front panel is responsible for displaying the results.

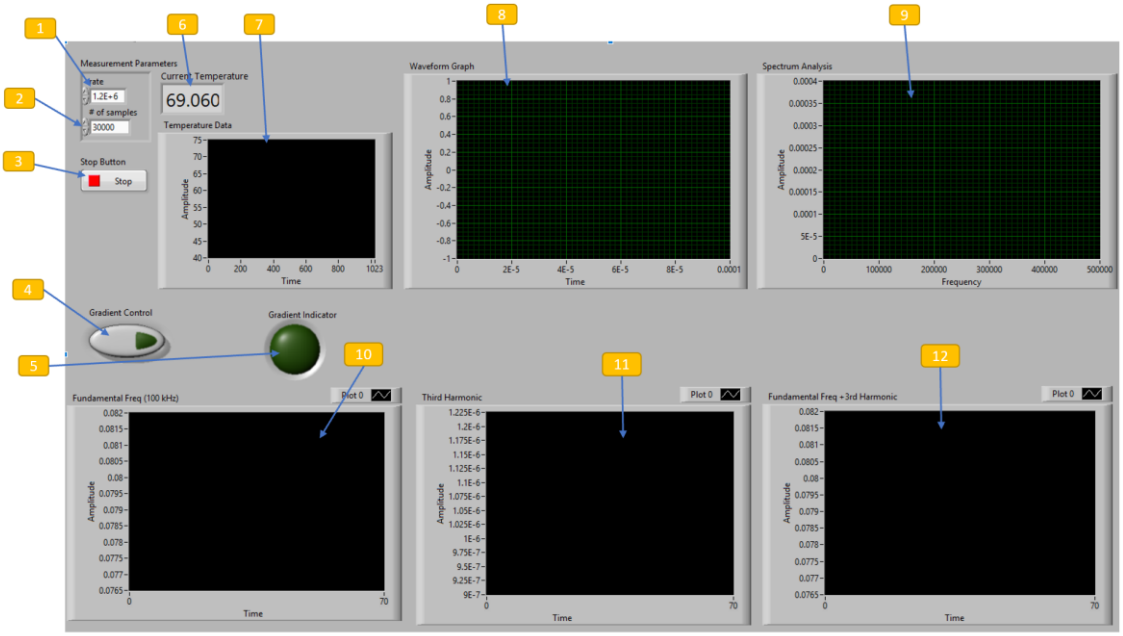

Figure 40. LabVIEW front panel

(1) Sampling rate provides the acquisition rate of the DAQ.

(2) Number of Samples provides the number of samples per measurement. The total time per measurement is sampling rate multiplied by the number of samples.

(3) The Stop Button halts the experiment.

(4) Gradient Control button turns the gradients on and off.

(5) Gradient Indicator turns on when the gradients are too hot.

(6) Temperature (°C) displays the average temperature from the thermocouples.

(7) Temperature data plots the temperature reading for each measurement.

(8) The Signal Output (time) graph plots the signal from the receive coil in the time domain.

(9) The Signal Output (Frequency) graph plots the signal from the receive coil in the frequency domain.

(10) Fundamental frequency graph plots the signal at the fundamental frequency with each measurement.

(11) Third harmonic graph plots the signal at the third harmonic with each measurement.

(12) Fundamental frequency added to third harmonic graph plots the sum of the two harmonics for each measurement.

CHAPTER III

SYSTEM ANALYSIS

III.1 Signal Processing in LabVIEW

Signal processing is critical to determining the noise level of our system. The lower the noise level, the lower the concentration of particles the system can detect. One of the most critical signal processing portions of LabVIEW was determining which fast Fourier transform function to use. Initially, the FFT Spectrum (Mag-Phase).vi,  , was used to analyze the frequency content of the time signal. However, the algorithm of this function resulted in a high noise floor level. Upon some trial and error, the FFT Power Spectrum and PSD.vi,  , was used to analyze the frequency content of the signal. The noise floor due to the signal processing of each function was easily tested by terminating the DAQ system with a 50Ω load with a transmission line. As seen from Figure 41, the noise baseline in the frequency domain is approximately 1.75×10^{-6} while using the FFT Spectrum (Mag-Phase).vi. The noise baseline in the frequency domain is approximately 1.5×10^{-11} while using the FFT Power Spectrum and PSD.vi as seen in Figure 42.

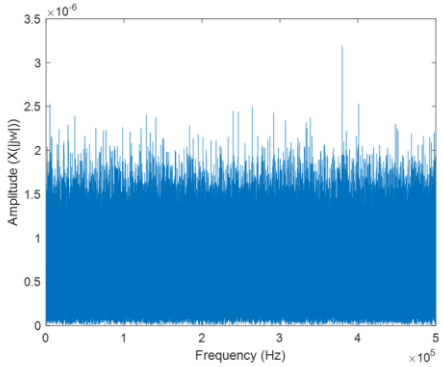

Figure 41. The frequency spectrum generated using the FFT Spectrum (Mag-Phase).vi. The baseline noise level is approximately 1.75 x 10^{-6}.

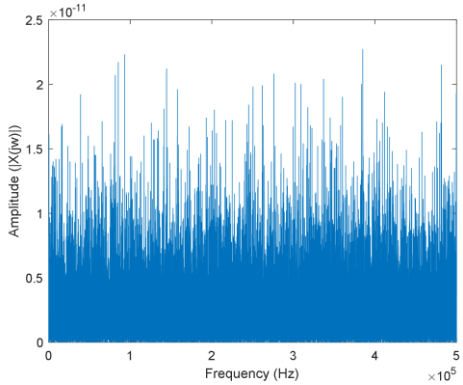

Figure 42. The frequency spectrum generated using the FFT Power Spectrum and PSD.vi. The baseline noise level is approximately 1.5 x 10^{-11}.

III.2 Noise Analysis of System

A low noise system will directly affect the sensitivity of the system. In this section, noise measurements will be measured for each system component. The following is the procedure for the noise analysis of the system:

(1) Test the DAQ with the cable terminated with 50 ohms. Save the frequency and time domain response.

(2) Test the DAQ with the cable and the LNA terminated with 50 ohms. Set the DC power supply to 13.4 V. Save the frequency and time domain response.

Terminate input of LNA with 50 ohms

(3) Test the DAQ with the cable, LNA, and receive coil. Place the receive coil in the transmit coil. Save the frequency and time domain response.

(4) Test the DAQ with the cable, LNA, and receive coil. Leave the receive coil in the transmit coil. Connect the power amplifier to the waveform generator. Turn on the power amplifier, but not the waveform generator. The power amplifier is terminated with 50 ohms. Save the frequency and time domain response.

(5) Turn on the waveform generator. Set the frequency to 100 kHz and amplitude to 0.5 Vpp to power the transmit coil. Save the frequency and time domain response.

(6) Now place the transmit coil and receive coil fixtures inside the gradient coil. Connect the receive chain and transmit chain to the brass tube using the connectors at the end. Connect the receive coil to the rest the receive chain through the connectors on the inside-end of the brass tube but leave the transmit coil unconnected. Save the frequency and time domain response.

(7) Connect the transmit coil to the end of the gradient coil. Do not power on the transmit coil. Save frequency and time domain response.

(8) Turn on the waveform generator and power amplifier to power the transmit coil. Save the frequency and time domain response.

From step (1):

The results as shown in Figure 43. The noise floor is approximately 1.25 x 10^{-11}.

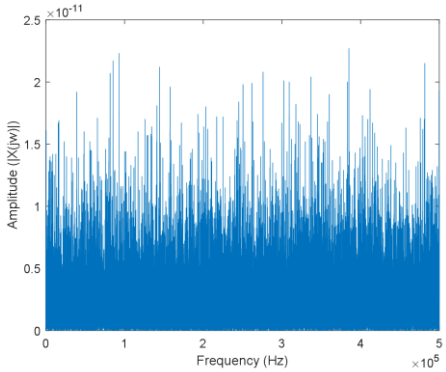

Figure 43. Step (1). The signal received from the DAQ with the DAQ terminated with 50 Ω.

From step (2):

The results are shown in Figure 44. The noise floor is approximately 2 x 10^{-11}.

This was expected due to the LNA. However, the additional frequency spikes around 1.2 kHz, 2.3 kHz, 3.3 kHz and 4.4 kHz were not expected.

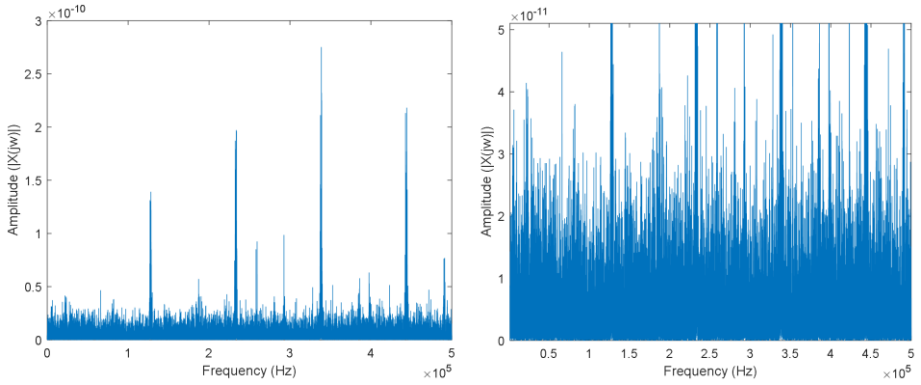

Figure 44. Step (2) Right picture: zoom in of figure on the left. Test the DAQ with the cable and the LNA terminated with 50 ohms. Set the DC power supply to 9.4 V.

From step (3):

The results are shown in Figure 45. The noise baseline was not as consist with a noise baseline of approximately 8 x 10^{-11}. At this point the receive coil has been placed in the transmit coil. However, everything is off on the transmit side. However, this indicates that the receive coil is still picking up some ambient noise.

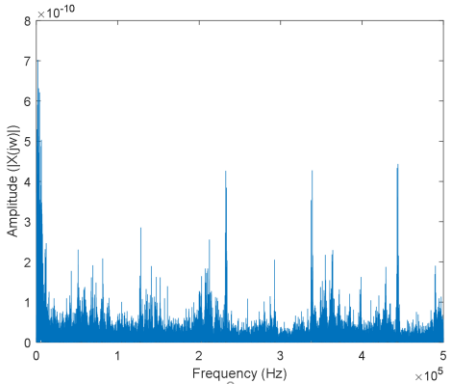

Figure 45. Step (3) Test the DAQ with the cable, LNA, and receive coil. Place the receive coil in the transmit coil.

From step (4):

The results are shown in Figure 46. The noise baseline has approximately stayed the same at approximately 8 x 10^{-11}. However, some of the frequencies have been amplified. This is potentially due to the power amplifier being on and some leakage current being picked up by the receive coil and being amplifier by the LNA.

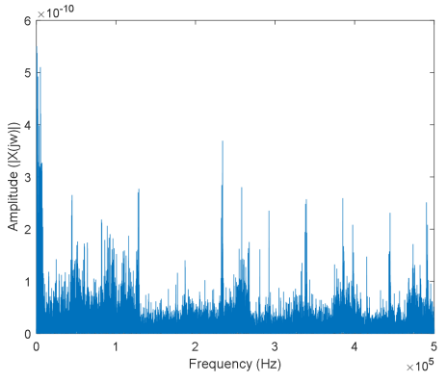

Figure 46. Step (4) Test the DAQ with the cable, LNA, and receive coil. The receive coil was left in the transmit coil. The power amplifier was connected to the waveform generator. The power amplifier was turned on, but not the waveform generator. The power amplifier was terminated with 50 ohms.

From step (5):

The results are shown in Figure 47. The noise baseline was approximately 8×10^{-11}. Since the transmit coil is powered, the fundamental frequency is present. The second harmonic was present as well; however, it is approximately -30 dB lower than the fundamental frequency. The fundamental and the successive harmonics will be limiting factors for the sensitivity of the system.

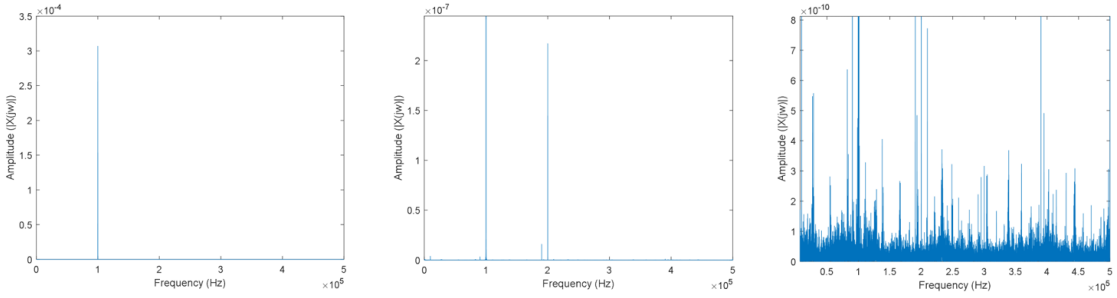

Figure 47. Step (5) The waveform generator was turned on. The frequency was set to 100 kHz and amplitude to 0.5 Vpp to power the transmit coil.

From step (6):

The results are shown in Figure 48. The noise baseline was approximately 4×10^{-11}. The decrease in noise baseline is expected since the transmit coil is turned off. Compared to the receive coil when it is not grounded to the gradient coil in step (3), the noise level is lower in step (6), which is expected because the brass tube acts like a shield for the receive coil.

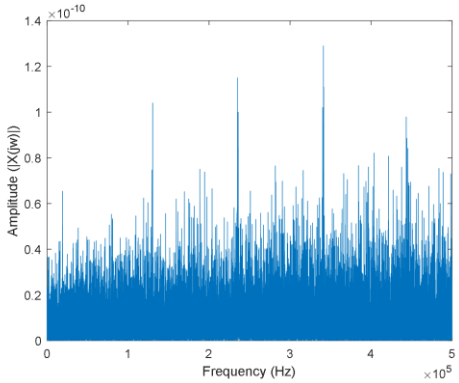

Figure 48. Step (6) the transmit coil and receive coil fixtures were placed inside the gradient coil. The receive chain and transmit chain were connected to the brass rod using the connectors at the end.

From step (7):

The results are seen in Figure 49. The noise baseline is approximately 1×10^{-11}. The noise baseline is low with none of the spurious harmonics being higher than 9 x 10^{-10}. This indicates that the brass rod is providing a good ground and shield to both the transmit coil and receive coil.

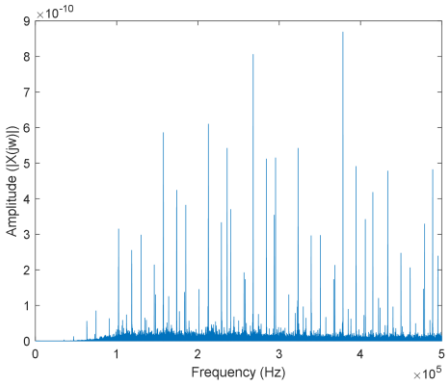

Figure 49. Step (7) The transmit coil was connected to the end of the gradient coil. The transmit coil was not turned on.

From step (8):

The results were shown in Figure 50. The LNA amplified the fundamental frequency in addition to the harmonics. Without any decoupling the fundamental frequency would dominate the signal, and no particles could be detected. Decoupling the transmit coil and receive coil will be discussed in Section III.3. The noise baseline for the fundamental frequency and the associated harmonics are 0.3, 0.004 and 0.003 respectively. The noise baseline for the system overall with the LNA included was approximately 5 x 10^{-9}.

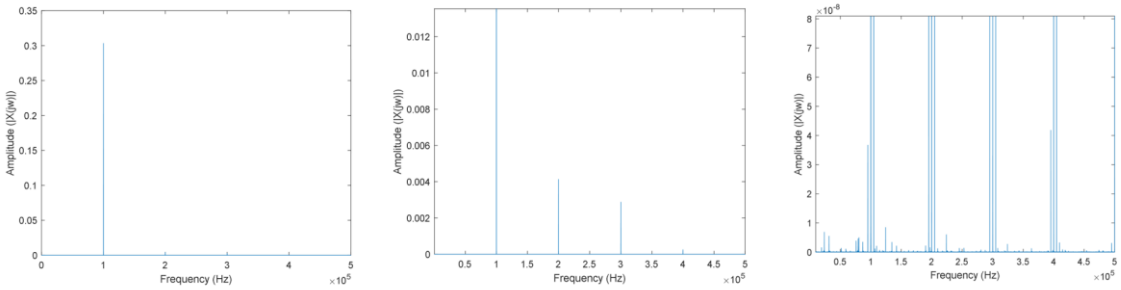

Figure 50. Step (8). Baseline signal with LNA included (left). Baseline signal with LNA included. Zoomed in to second and third harmonic (middle). Spurious harmonics begins to form around the relevant harmonics. The noise baseline is around 5 x 10^{-9} (right).

The noise baseline using the NI DAQ 6353 was 1.25 x 10^{-11}. Therefore, if the entire MPI system was able to achieve a noise baseline close to this magnitude, then a new DAQ should be considered. Once the LNA was inserted into the system, the noise floor did not change much; however, the LNA introduced frequency spikes on an order of magnitude from the noise floor. While this is not much, there is currently no signal going into the LNA. Once a signal goes into the LNA, the LNA may unevenly amplify frequencies. To improve the SNR of the system, a better LNA may be considered. There are some noise contributions from including the receive coil and transmit coil. However, since the transmit coil is grounded with the brass tube, it acts like a shield for the coils.

III.3 Transmit Coil and Receive Coil Isolation

In order to keep the fundamental frequency as part of the signal response from the particles, the transmit coil and the receive coil need to be decoupled. If the receive coil picks up a large portion of the fundamental frequency from the transmit coil, then the fundamental frequency must be filtered out. Otherwise, the fundamental frequency will oversaturate the LNA as seen in Figure 51.

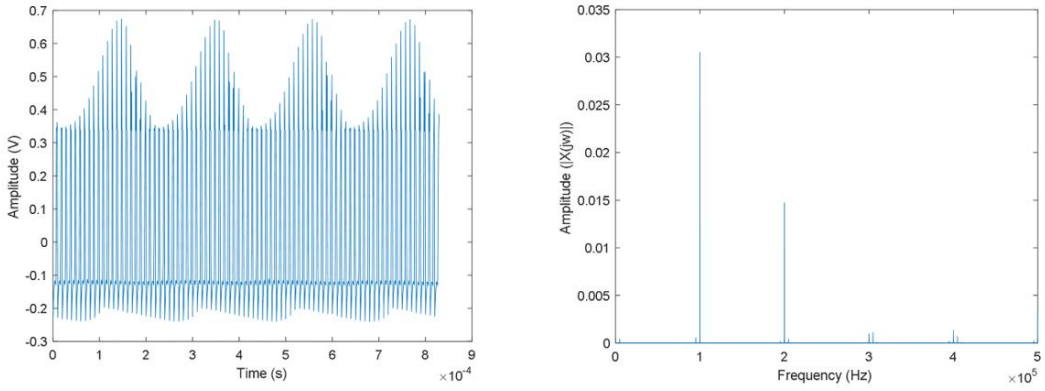

Figure 51. The whole MPI system is connected and the transmit coil and receive coil are inside the gradient coil. Time domain (left). Frequency domain (right)

We can see erratic behavior in the time domain and spurious emissions in the frequency domain. Therefore, it is critical to decouple the transmit coil and receive coil to drive down the fundamental frequency picked up by the receive coil.

In order to decouple the transmit coil and receive coil, the receive coil will be a gradiometer configuration and will position itself in respect to the transmit coil to achieve the best decoupling possible. Decoupling the transmit coil and receive coil takes a bit of experience, patience, and luck.

The first step to decoupling the transmit coil and receive coil is to take out the LNA. The LNA will amplify all frequencies and if it oversaturates, it becomes a non-linear system, which makes it even more difficult to decouple the transmit coil and receive coil. Without the LNA, position the transmit coil and receive coil in respect to each other until there is the least amount of coupling between the two coils as seen in Figure 52.

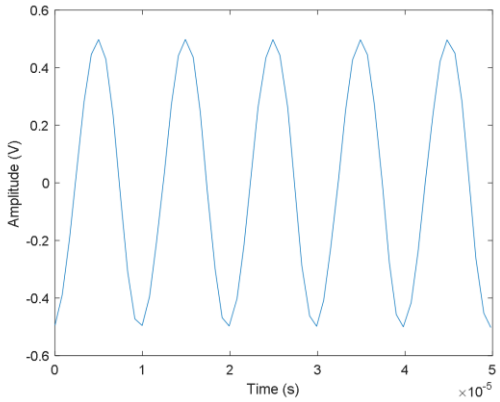

Figure 52. Signal between the transmit coil and receive coil after decoupling.

Once the highest decoupling has been achieved between the two coils, reintroduce the LNA back into the system. More likely than not, the transmit coil and

receive coil will need to be tweaked even further. As shown in Figure 53, harmonics are present at a high level even though there are no particles in the receive coil.

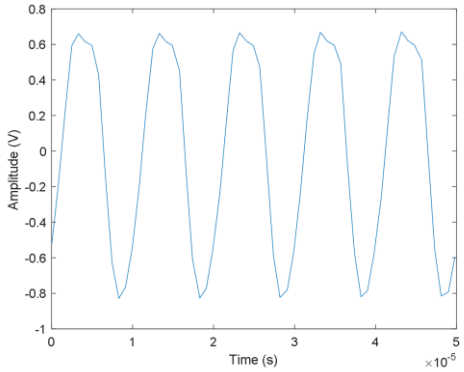

Figure 53. Time response after reintroducing the LNA back into the system.

Therefore, the two coils must be further decoupled by slightly tweaking the position of the receive coil in respect to the transmit coil. After a lot of tiny adjustments, the best isolation achieved between the receive coil and transmit coil achieved was approximately 0.3 V_{pp} and the fundamental frequency at 0.011 as shown in Figure 54. After decoupling the two coils, less harmonics are seen both in the time domain and frequency domain. In addition, the V_{pp} is much lower.

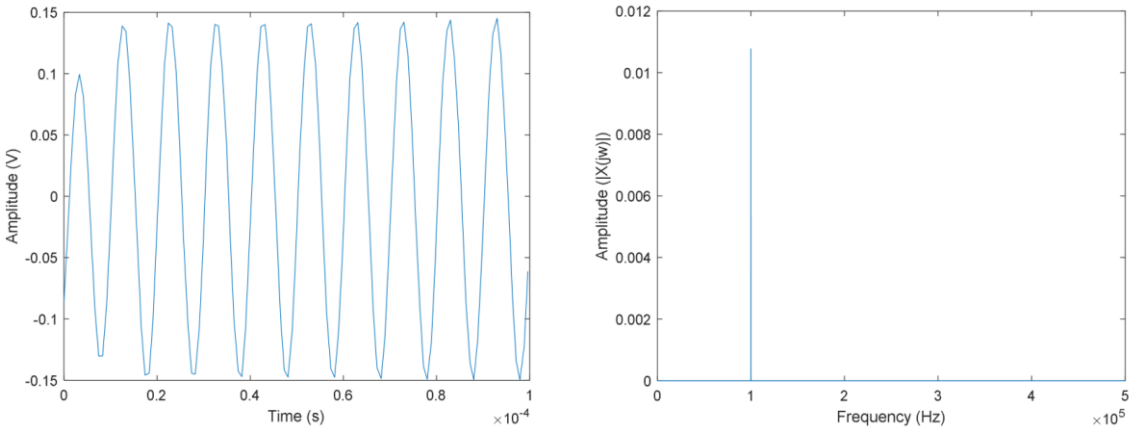

Figure 54. Time domain (left) and frequency domain (right) of a decoupled transmit coil and receive coil.

III.4 Baseline Fundamental Frequency and Third Harmonic Analysis

Upon closer inspection, we noticed that the baseline fundamental frequency amplitude would change over time. In order to isolate the source of the problem, the amplitude of the fundamental frequency and third harmonic over time was recorded as shown in Figure 55 which shows that the DAQ has a relatively stable baseline fundamental frequency and third harmonic.

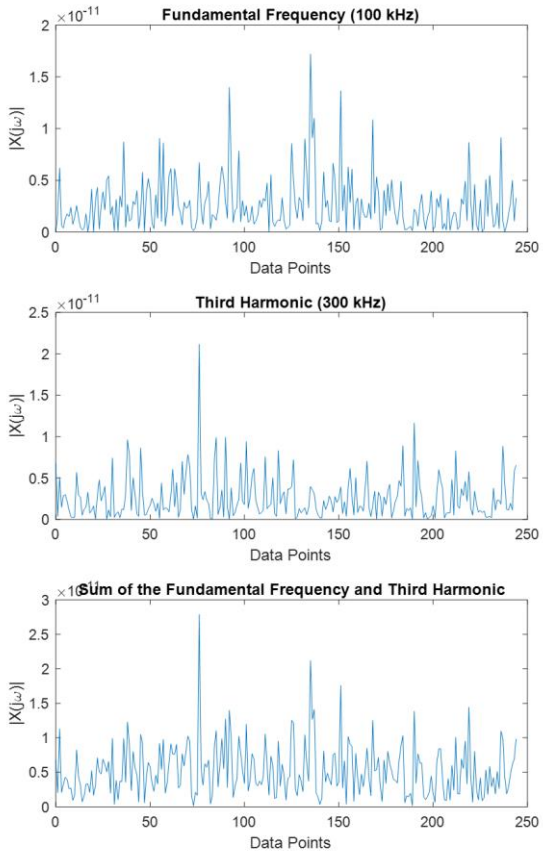

Figure 55. (Top) Fundamental Frequency (Middle) Third Harmonic (Bottom) Sum of the fundamental and third harmonic. The baseline signal with DAQ terminated with 50 ohm input was relatively stable. There were no signs of an increasing baseline.

Next, the waveform generator was connected directly to the DAQ. The results of the fundamental frequency and third harmonic are shown in Figure 56. Again, the fundamental frequency and third harmonic signal from the waveform generator into the DAQ was relatively stable.

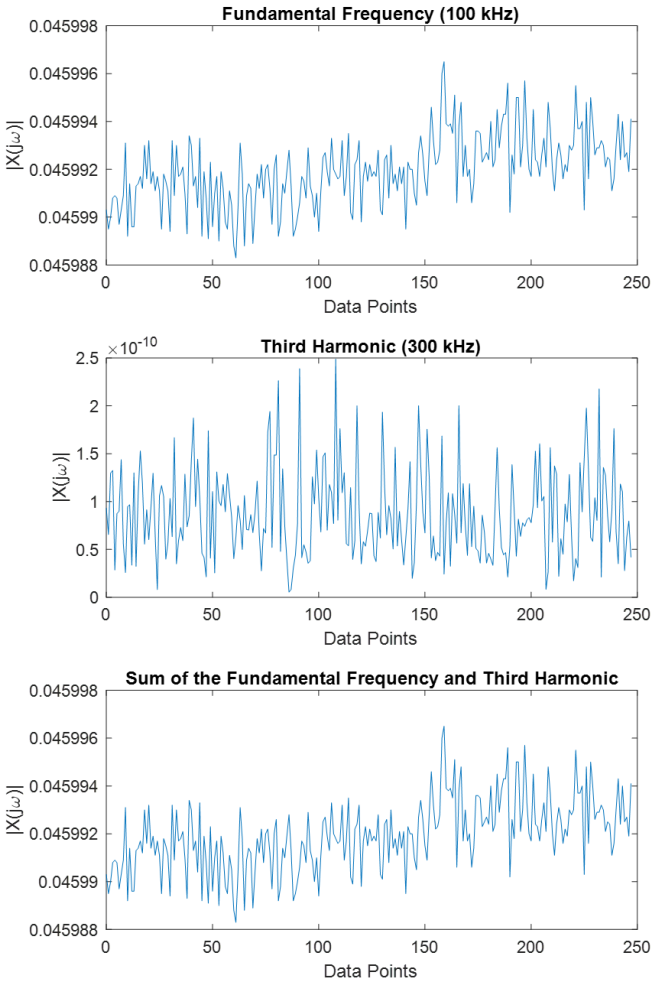

Figure 56. (Top) Fundamental Frequency (Middle) Third Harmonic (Bottom) Sum of the fundamental and third harmonic. The baseline signal with the waveform generator directly input into the DAQ seemed relatively stable. There were no signs of the baseline levels increasing over time.

Now, the waveform generator was connected to the power amplifier. The signal was then attenuated with a -30 dB attenuator and then connected to the DAQ. From

Figure 57, the power amplifier is also relatively stable. However, this is somewhat inconclusive since there is a -30 dB attenuator which could diminish the magnitude of the change in the baseline.

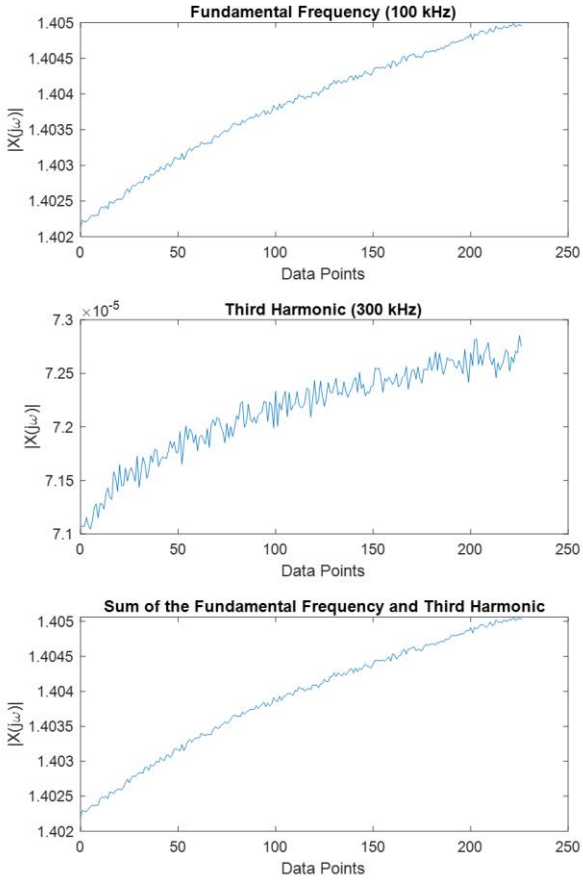

Figure 57. (Top) Fundamental Frequency (Middle) Third Harmonic (Bottom) Sum of the fundamental and third harmonic. The baseline signal with the power amplifier steadily increased over time.

III.5 Gradient Coil Testing

III.5.1 Gradient Strength

The gradient was powered using the Power Ten Inc. Model P 66 Series. The voltage on the power supply was set to 161 V and 10 A. The DC Gaussmeter Model 1

Hall probe (AlphaLab Inc.) was used to measure the magnetic field inside the gradient coil. The hall probe was positioned using the millimeter positioner. The equipment used are shown in Figure 58**.**

Figure 58. (Left) The Power Ten Inc. Model P 66 Series power supply. (Right) The DC Gaussmeter Model 1 Hall probe.

The hall probe was placed approximately in the center position of the gradient coil. Since the dynamic region of the gradient coil is in the space between the two coils, the hall probe was placed slightly inside the inner edge of the gradient coil as shown in Figure 59 . Be careful when testing the gradient coil. Make sure to turn it off between each measurement. The gradient coils get hot very fast. The results are summarized in Table 8.

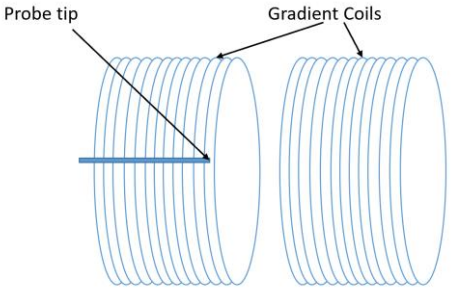

Figure 59. An illustration of the gradient coil and probe starting placement for characterizing the gradient strength.

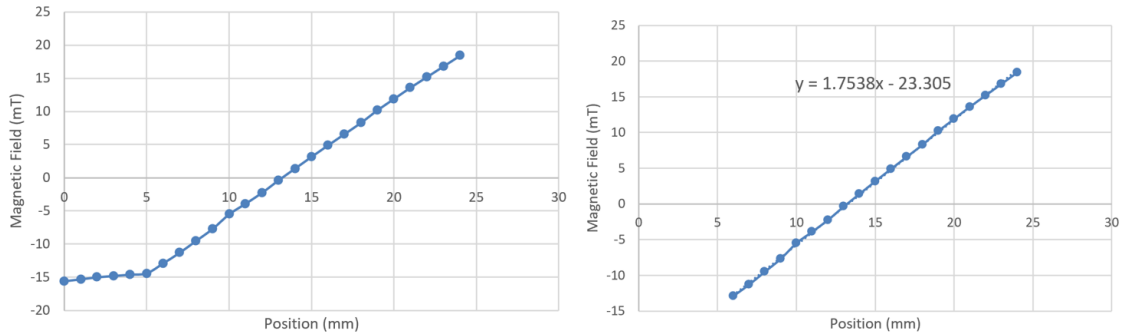

Figure 60. (Left) All the data points collected inside the center line of the gradient coil. (Right) The points used to extrapolate the gradient field. At 10 A, the gradient coil produced 1.75 mT/mm which is slightly below the 2 mT/mm simulated results.

Position (mm)	Magnetic Field (Gauss)	Magnetic Field (tesla)
0	-156	-0.0156
1	-153	-0.0153
2	-150	-0.015
3	-148	-0.0148
4	-146	-0.0146
5	-144	-0.0144
6	-129	-0.0129
7	-113	-0.0113
8	-95	-0.0095
9	-77	-0.0077
10	-55	-0.0055
11	-39	-0.0039
12	-22.5	-0.00225
13	-3.7	-0.00037
14	14	0.0014
15	31.7	0.00317
16	49	0.0049
17	66	0.0066
18	83	0.0083
19	102	0.0102
20	119	0.0119
21	136	0.0136
22	152	0.0152
23	168	0.0168
24	184	0.0184

Table 8. Summary of the magnetic field inside the gradient coil in respect to position. (Power supply settings: 161 V and 10 A)

Position (mm)	Magnetic Field (Gauss)	Magnetic Field (tesla)
0	-156	-0.0156
1	-153	-0.0153
2	-150	-0.015
3	-148	-0.0148
4	-146	-0.0146
5	-144	-0.0144
6	-129	-0.0129
7	-113	-0.0113
8	-95	-0.0095
9	-77	-0.0077
10	-55	-0.0055
11	-39	-0.0039
12	-22.5	-0.00225
13	-3.7	-0.00037
14	14	0.0014
15	31.7	0.00317
16	49	0.0049
17	66	0.0066
18	83	0.0083
19	102	0.0102
20	119	0.0119
21	136	0.0136
22	152	0.0152
23	168	0.0168
24	184	0.0184

Table 8 continued.

At 10 A, the gradient coil produced 1.75 mT/mm. Therefore, the gradient produces a gradient strength of 0.175 mT/mm•A.

III.5.2 Gradient Heating

As current flows through the wire, some of the power is disputed as heat. Therefore, the gradient coil will heat up over time. Using the Omega T-type Thermocouple (SA1-T), the temperature of the gradient coil was measured. As shown in

Figure 61, over a span of two minutes the gradient coil increased by 20 °C. LabVIEW program as discussed in Section II.7 had a threshold temperature of 60 °C.

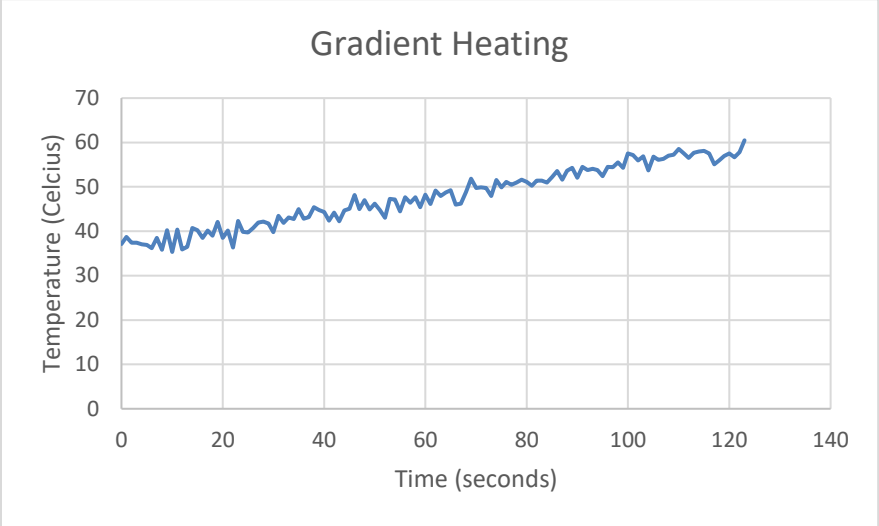

Figure 61. Gradient heating over a period of two minute

As seen from the figure, the gradient heats up quickly. In order to protect the gradient coil, LabVIEW was used to control the power supply through a D-type connector.

Using a fan to promote airflow and cooling, gradient cooling was also recorded as a function of time as shown in Figure 62.

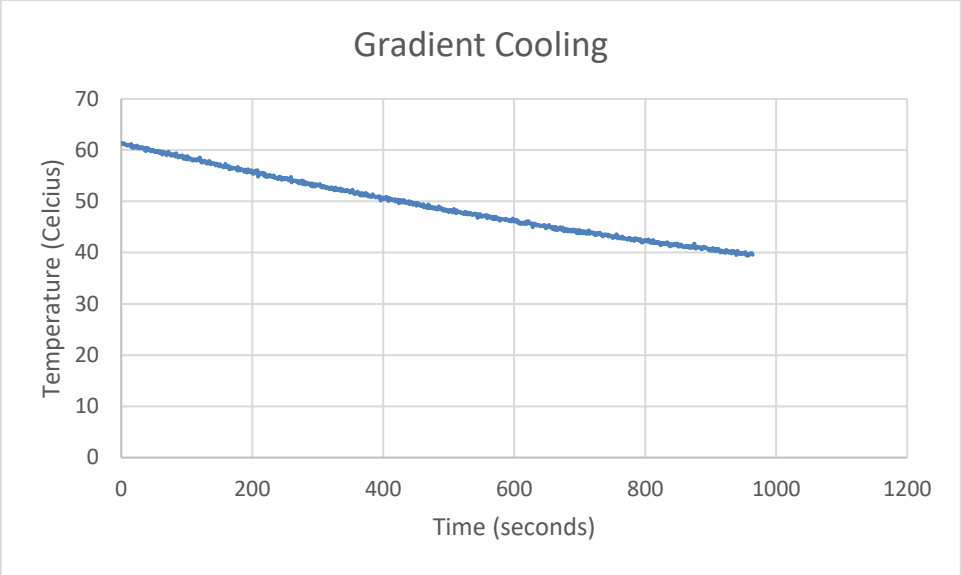

Figure 62. Gradient cooling over a period of approximately 16 minutes.

The gradient takes approximately 15 minutes to return to the original temperature. Therefore, it is highly advised that for the next iteration of this project, the gradients should have a duty cycle. One suggestion would to have the gradients on a 20% duty cycle with approximately 1 second to turn on, 2 seconds to take measurements, 1 second to turn off, and 6 seconds to rest.

III.6 Gradient Noise Analysis

In addition, the gradients contribute to the noise baseline. The noise contribution from the gradients are observed in Figure 63. The gradients increased the noise baseline by 0.01196 in the fundamental frequency and 8.63×10^{-7} in the third harmonic. That is approximately 14% increase noise baseline for the fundamental frequency and approximately 50% increase noise baseline for the third harmonic.

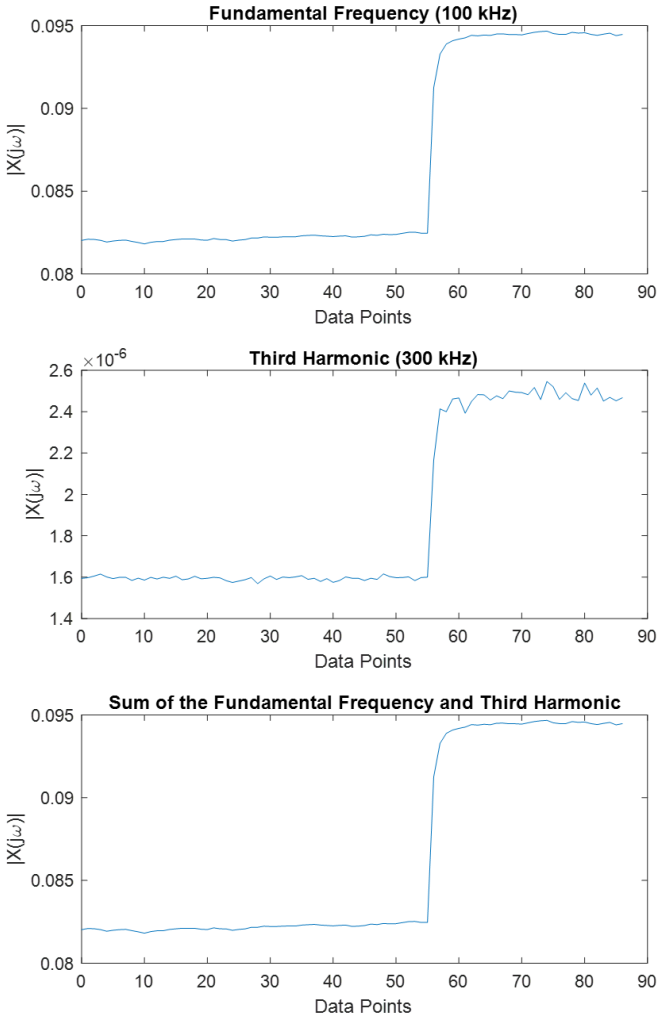

Figure 63. (Top) Fundamental frequency (Middle) Third Harmonic (Bottom) Sum of the fundamental frequency and third harmonic. The gradient was turned on at data point 56. The gradients increase the noise baseline.

The drastic increase in the noise baseline by the gradient coil severely limits the sensitivity level of the MPI system. This increase in the noise baseline is potentially caused by eddy currents generated on the surface of the brass tube which will then affect the transmit coil and receive coil. Eddy currents are caused by a changing magnetic field due to Faraday's law of induction. Eddy currents are loops of currents that occur mainly

on the surface of the conductor. These loops of current will in return induce a magnetic field which will affect the transmit coil and receive coil.

III.7 Potentially Helpful Tips

III.7.1 Gradient Heating

Gradient heating is a big issue. After just about 60 seconds, the temperature can rise by 10 °C. A few ways to address this issue are to have a fan to circulate the air in and around the gradient coil, including a heat sink to the gradient coil, and having a duty cycle for the gradient coil.

III.7.2 Designing the Matching/Tuning Network

While designing the matching/tuning network by using the Smith v4.1 software may be straightforward, the actual implementation may be difficult. When the transmit coil and receive coil were first built, the transmit coil needs to be matched and tuned in order to if the receive coil can detect particles. However, once the transmit coil and receive coil are included into the gradient coil system, this will change the magnetic environment. As a result, the matching/tuning network will need to be modified to account for this change.

III.7.3 Coil Fixture

The coil fixture is a critical component of housing the transmit coil and receive coil in addition to isolating and decoupling the transmit and receive. The coil fixtures were printed using PETG. However, after running the system, the transmit coil fixture has slightly warped. This could be due to the heat generated from the transmit coil in

addition to the gradient coil heating. Therefore, in future iterations of the coil fixture, resin or a more thermally resistant material should be used.

III.7.4 Transmit Coil and Excitation Field

Decoupling the transmit coil and the receive coil is an extremely challenging feat, especially if the fundamental frequency is going to be included in the imaging process. Often researchers will filter out the fundamental frequency since it contains too much of the excitation field. In this project, we attempted to preserve the fundamental frequency. However, this was difficult and later, it was realized that it may have been to slight variations of the magnetic field inside the transmit coil either due to the coil fixture having defects or the loops not being compacted together. In the future, make sure to keep the loops tight and close to ensure the solenoid is uniform.

III.7.5 System Error

Statistical analysis is a helpful way of determining the relevance of the data. One common method is to use error bars. Error bars are a data visualization method of plotting the variability in a data set. It is used to help determine statistical significance. While in this paper, error bars and statistical analysis were not implemented, it would be useful in the future.

There are a few reasons why statistical analyses were not considered in this paper, with the root cause being instability in the system. The transmit coil and receive coil are extremely position sensitive. Any sort of movement would distort the decoupling between the two coils which would increase the noise level. While movement between the transmit coil and receive coil in some cases were preventable such as using a holding

structure to fix the transmit coil and receive coil, others were unavoidable with the current setup such as the coil fixture expanding due to the heat from the coil. Another issue was the noise caused by the gradient and gradient heating. The gradient caused the noise baseline to increase drastically as discussed in Section III.6. Therefore, it was difficult to perform and discuss error analysis.

CHAPTER IV

TEST AND RESULTS

IV.1 Proof of Particles

A simple test was conducted to determine that the signal was due to the particles and not due to the perturbation between the receive coil and transmit coil when the SPIONs were introduced. The waveform generator was set to 20 mV_{pp} and a solid piece of metal was introduced into the bore of the receive coil. Next the SPIONs were introduced into the bore of the receive coil. Next, the waveform generator was set to 650 mV_{pp} and again the solid piece of metal was introduced into the bore of the receive coil and then the SPIONs were introduced into the bore of the receive coil.

The test was performed with a vial of 0.1cc of 25 nm SPIONs with a concentration of 5 mg/mL and a small screw as shown in Figure 64.

Figure 64. (Right) Small Screw (Left) 25 nm SPIONs, 5 mg/mL, 0.1 cc used to prove the MPI system is detecting particles.

As seen from Figure 65, the fundamental frequency changed while the third harmonic did not have any noticeable change when the waveform generator was set to 20 mV_{pp}. This was expected because at such low applied magnetic fields, the SPIONs are not pushed into the saturated region, but rather stay in the linear dynamic region (look at Figure 3). This will result in a change in the fundamental frequency but not in the third harmonic. When the waveform generator was set to 650 mV_{pp}, there is a noticeable change for both the fundamental frequency and the third harmonic which is expected when the SPION magnetization are in the saturated region.

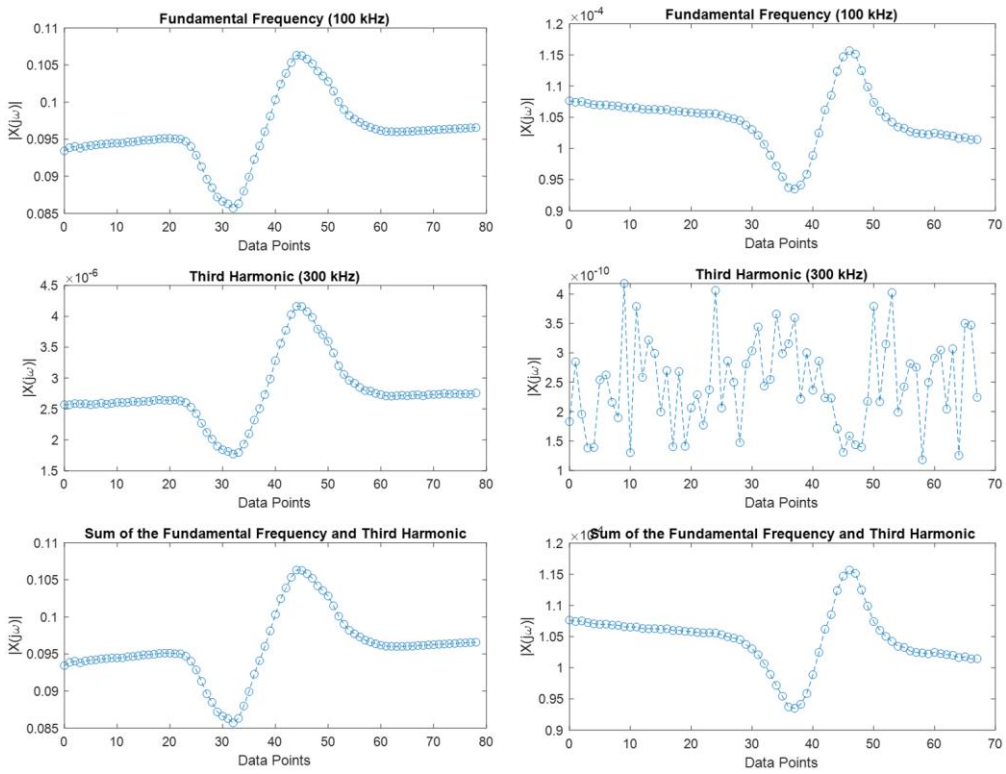

Figure 65. (Top row) Fundamental frequency (Middle row) Third harmonic (Bottom row) Fundamental frequency and third harmonic added together. (Left column) waveform generator set to 20 mVpp. (Right colum) waveform generator set to 650 mVpp. The sample was 25 nm SPIONs at 2.5 mg/mL and 0.1 cc.

As seen in Figure 66, both the fundamental frequency and third harmonic both have a noticeable change when the waveform generator was set to 20 mV_{pp} and 650 mV_{pp}. This is expected because the metal screw is a metal object. By introducing a metal object into the coils, this will perturb the magnetic environment and cause the receive coil to pick up this change in the magnetic environment. However, this is just the coupling between the transmit coil and receive coil. This will result in a change in the fundamental frequency and the third harmonic.

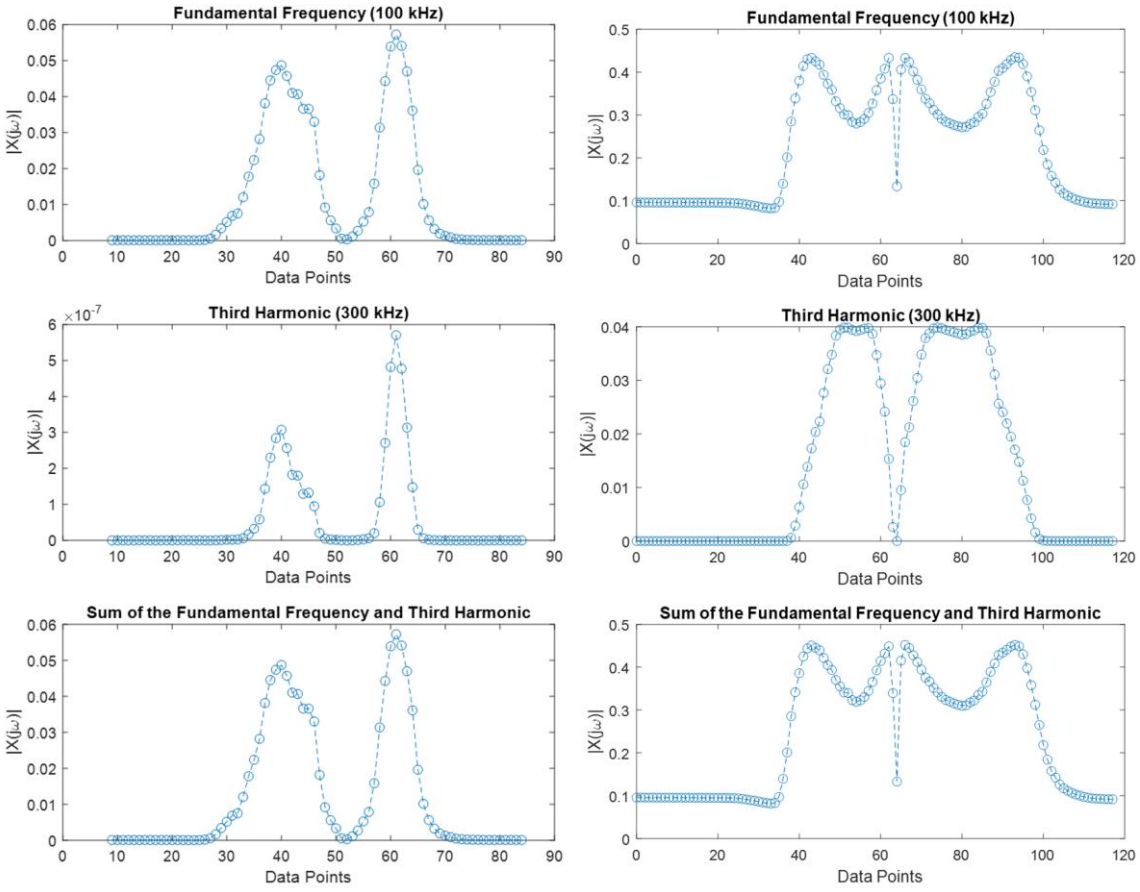

Figure 66. (Top row) Fundamental frequency (Middle row) Third harmonic (Bottom row) Fundamental frequency and third harmonic added together. (Left column) waveform generator set to 20 mVpp. (Right colum) waveform generator set to 650 mVpp. The sample was a small screw as shown in Figure 64.

To further show that the system is detecting particles, instead of using a magnetic object, copper, a non-magnetic metal, response is compared to the particles in the receive coil. The copper does elicit a similar response to the metal screw. This is expected since as the copper moves through a changing magnetic field, this will cause electrical currents to flow on the surface of the copper, also known as eddy currents. As briefly mentioned in Section III.6, eddy currents are circular flow of electrical currents that occur in a conductor due to an external magnetic field. The eddy currents will result in a changing magnetic field which will induce a voltage change (once again Faraday's law of induction) in the receive coil. Therefore, to show that the receive coil was detecting the SPIONs, the gradient was turned on, the waveform generator was set to 650 mV_{pp} to compare the SPION response and the copper response.

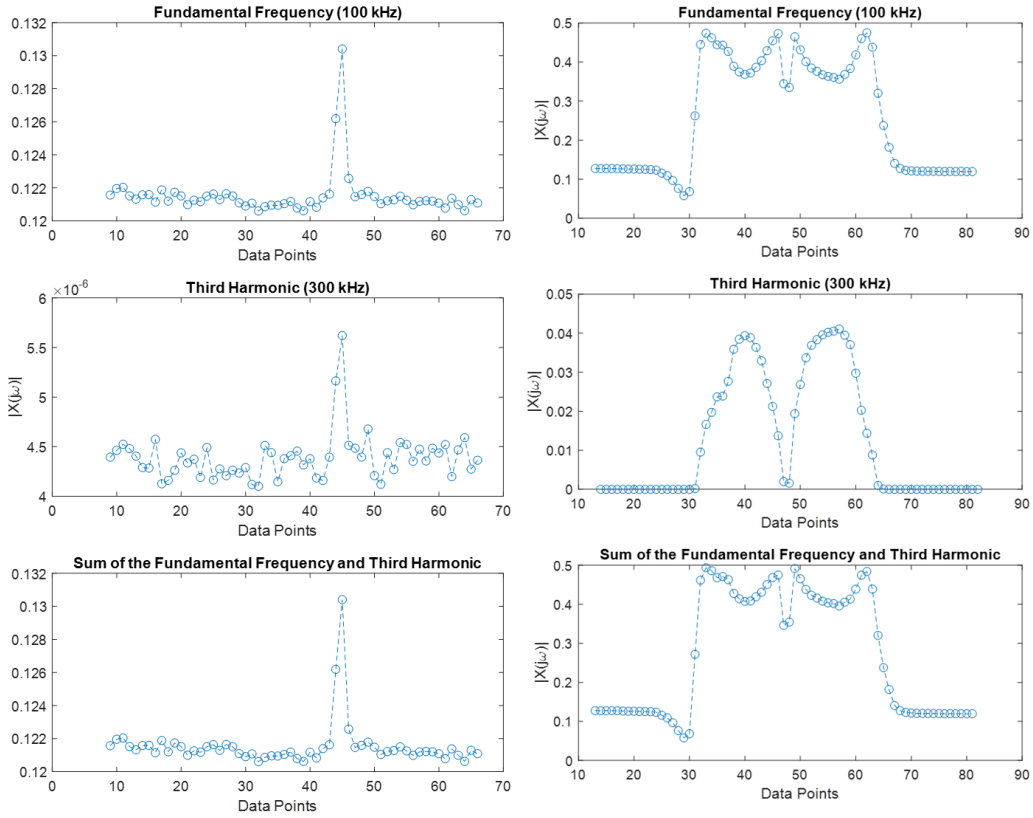

Figure 67. . (Top row) Fundamental frequency (Middle row) Third harmonic (Bottom row) Fundamental frequency and third harmonic added together. (Left column) SPION respone. (Right colum) Copper response. The plot shows that the particles are in saturation in the tuning loop while the copper is interacting with the tuning loop while the gradients are on.

As shown in Figure 67, the SPION had a response only in the signal pick-up loop. This proves that the particles are saturated in the tuning loop region by gradients, while their magnetization are changing in the signal pick-up loop region. The copper had four main peaks in the fundamental and two peaks in the third harmonic region. The first two peaks in the fundamental frequency were when the copper was passing through the tuning loop region and the second two peaks were when the copper was passing through

the signal pick-up loop region. This is expected from copper since the eddy currents will occur in the copper in both the tuning loop region and signal pick-up loop region.

Another method to proof that the system is detecting particles is by using the gradient. When the particles are inserted into the gradient, both the tuning loop and the signal pick-up loop will detect the particles. However, when the particles are inserted into the receive coil with the gradient on, the particles will only show up in the magnetic null region.

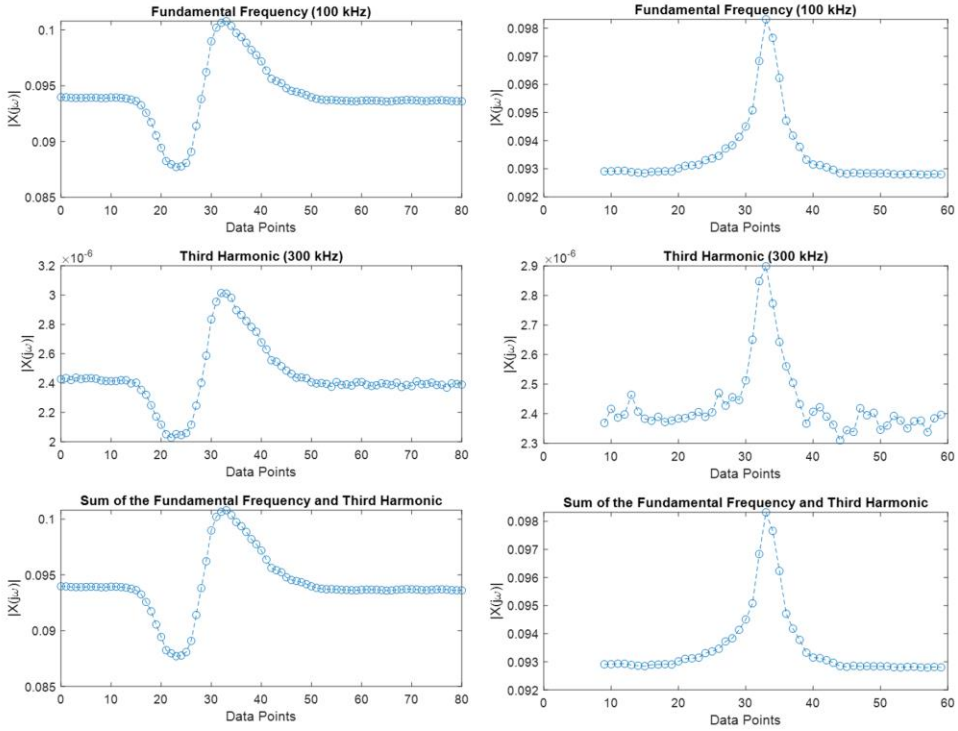

Figure 68. (Left Column) Gradient is off. (Right column) Gradient is on. The settings were 135 V and 6 A. (Top row) Fundamental frequency (Middle row) Third harmonic (Bottom row) Sum of fundamental frequency and third harmonic. This shows that the particles are in saturation when they are passing through the tuning loop.

Figure 68 displays the results of the particle response with and without the gradients. As seen in the left column, when the gradients are off, there is a decrease in

the signal and then a rise in the signal. The decrease is caused by the tuning loop having the opposite winding as the signal loop. Therefore, when the particles pass through the receive coil, the tuning loop will pick up the changing in magnetization in the particles and when the particles pass through the signal pick-up portion of the receive coil, the signal will increase. Now when the gradient is turned on, the magnetic region where the tuning loop will cause the SPIONs to be in saturation. Therefore, there will be no signal as the particles are passing through the tuning loop. However, the signal pick-up loop will be in the magnetic null region. Therefore, when the SPIONs are passing through the signal pick-up region, the particles will experience a change in magnetization.

IV.2 Magnetic Particle Relaxometry Detection Limit

IV.2.1 Sensitivity Analysis

The detection limit of the MPI system is critical to the sensitivity and resolution of the system. Before starting to test the entire system with the gradient, the sensitivity of the transmit coil and receive coil (also known as relaxometry) must be measured first.

A hole was drilled into a long acrylic rod to hold the vial. The acrylic rod was then carefully placed into the receive coil and placed on the millimeter positioner. Then the acrylic rod was moved forward until the peak signal was found. Only one vial was placed inside the receive coil each time since if multiple samples were placed the receive coil would pick up the additional sample as well. Remember this was to test the sensitivity of the transmit coil and receive coil without the gradient coil. Six vials with their respective volumes are summarized in Table 9. Twenty nanometer SPIONs and 2.5 mg/ml concentration were used in each vile.

Vial	Volume
1	0.02 ml
2	0.05 ml
3	0.1 ml
4	0.15 ml
5	0.2 ml
6	0.25 ml

Table 9. Summary of the volumes in each vile. 20 nm SPIONs and 2.5 mg/ml concentration were used in each vial.

Figure 69 displays the signal response from each vial and Table 10 summarizes the peak values at each vile for the fundamental frequency, second harmonic, and third harmonic. The noise baseline for the fundamental frequency was approximately 0.01428. The noise baseline for the second harmonic was approximately 8×10^{-6}. The noise baseline for the third harmonic was approximately 7.17×10^{-9}. Also notice that the signal dips before it starts to rise for each sample. This is due to the sample first moving through the tuning loop and then finally entering the signal pick-up loop.

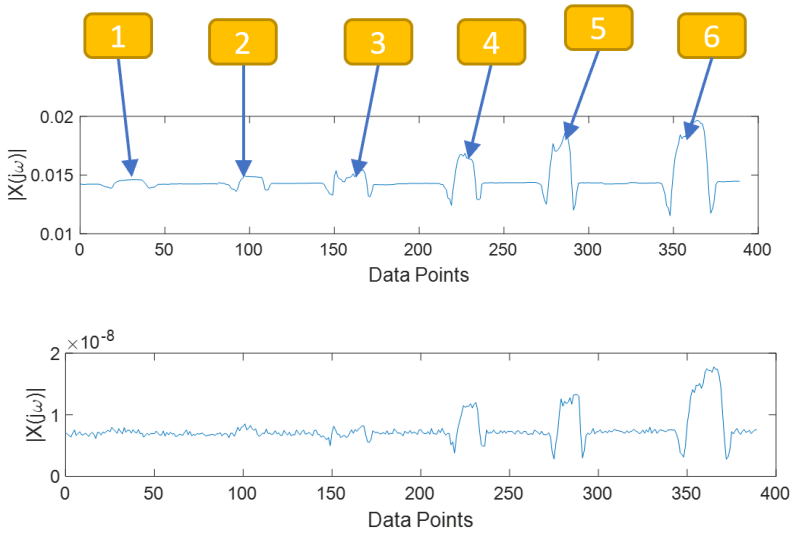

Figure 69. (Top) The fundamental frequency. (Bottom) Third Harmonic. (1) 0.02 ml. (2) 0.05 ml. (3) 0.1 ml (4) 0.15 ml (5) 0.2 ml (6) 0.25 ml. The noise baseline for the fundamental frequency was approximately 0.01428. The noise baseline for the third harmonic was approximately 7.17 x 10^{-9}.

Vial	Volume	Signal at 100 kHz	SNR at 100 kHz	Signal at 300 kHz	SNR at 300 kHz
1	0.02 ml	0.0146	1.02	N/A	N/A
2	0.05 ml	0.015	1.05	N/A	N/A
3	0.1 ml	0.01538	1.08	8.14E-09	1.14
4	0.15 ml	0.01675	1.17	1.18E-08	1.65
5	0.2 ml	0.01856	1.30	1.33E-08	1.85
6	0.25 ml	0.01948	1.36	1.75E-08	2.44

Table 10. Summary of the peak values at the third harmonic for each vial.

The signal to noise ratio (SNR) was calculated by dividing the signal to the noise baseline. Due to the low volume and low concentration (2.5 mg/ml), the SNR hovers around two for 0.25 ml.

IV.3 MPI Detection Limit

IV.3.1 Resolution Analysis

The resolution of the MPI system was by analyzed by placing two samples with the same concentration, particle size, and volume and separating them at various spacings. The spacing was defined as edge to edge as shown in .

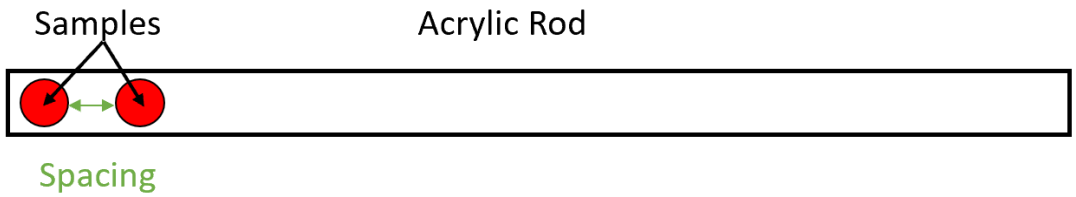

Figure 70. Illustration of spacing for resolution analysis.

25 nm particles with a concentration of 5 mg/mL and 0.1 mL volume were used for this experiment.

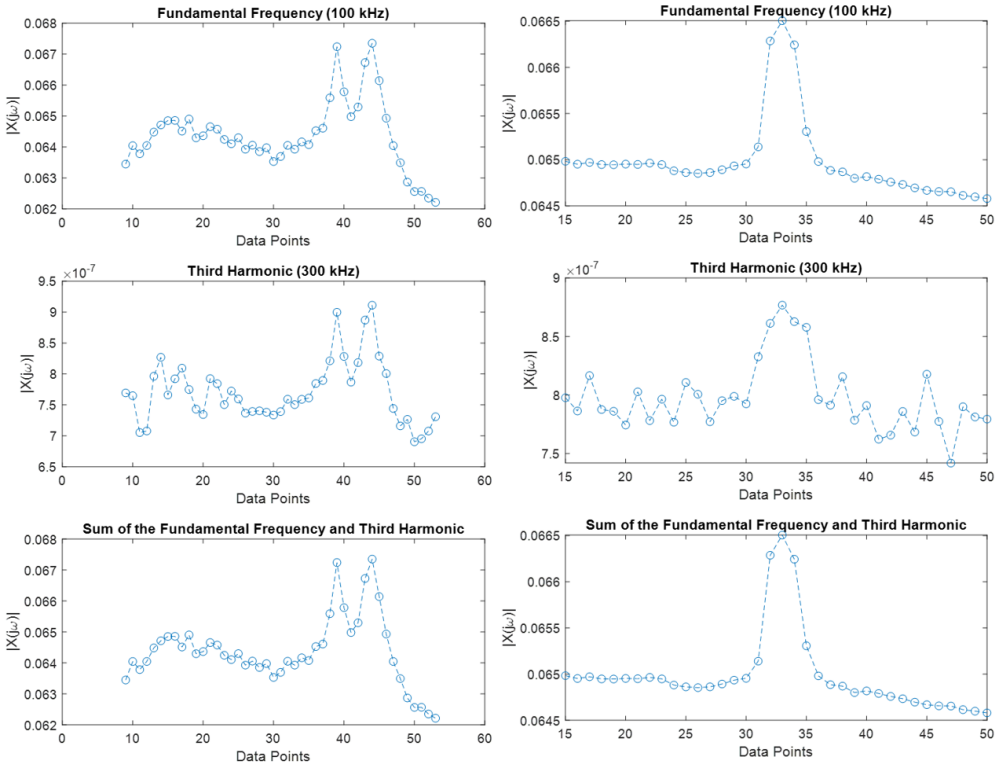

Figure 71. (Left Column) Samples separated by 5.3 mm (Right Column) Samples are separated by 2.51 mm. The gradient power supply was set to 160 V and 10 A.

As seen in Figure 71, with 10 A, the resolution of the system is approximately 5.3 mm. The two peaks can be seen clearly when the samples are separated by 5.3 mm; however, when the samples are separated by 2.51 mm, the two peaks are indistinguishable. However, according to the SPIO.m (Appendix F**Error! Reference source not found.**), with a gradient strength of 1.75 mT/mm, the system should have a resolution of 2.5 mm. Therefore, the system is off by a multiple of 2 for the expected resolution. One possible explanation is that the field free region is slanted due to the manufacturing of the gradient coil. Therefore, instead of a perfect plane, the gradient coil is producing a slanted plane which will affect the expected resolution of the system.

There are a couple ways to adjust the potential inhomogeneity of the gradient field. First, a map of the gradient field must be measured in order to find the magnetic field over the field free plane. Then, a bias coil can be implemented on top of the gradient coil in order to try and produce a homogenous magnetic field in the desired field free plane.

IV.3.2 Re-evaluation of resolution using new particles from Ocean Nanotech

We were able to acquire some 25 nm particles tailored for MPI from Ocean Nanotech. In this section, we will compare the 25 nm particles previously purchased from Ocean Nanotech to the newly acquired 25 nm particles, also from Ocean Nanotech. Two 0.1 mL vials for the new particles and two 0.1 mL vials of the old particles were spaced 2.5 mm apart. The particles were placed with the gradients on. The results of the experiment are displayed in Figure 72.

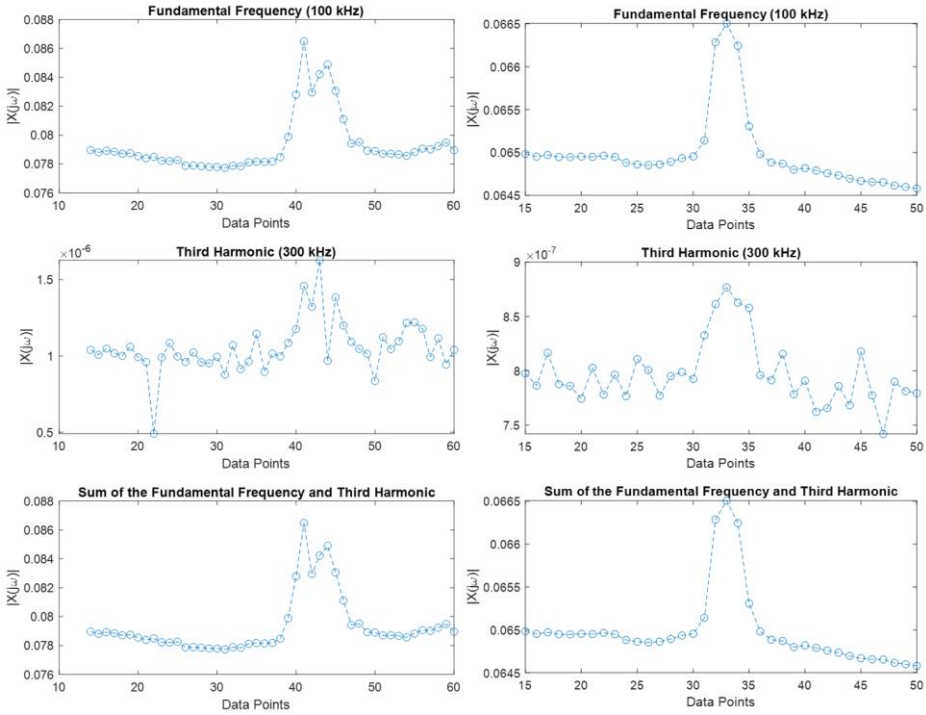

Figure 72. (Left column) New particles (Right column) Old particles. The comparison suggests that the new particles have a better signal response than the older particles as indicated by the two distinguishable peaks from the new particles and one peak from the old particles.

The new particles have a better magnetization response than the older particles as indicated by the two distinguishable peaks in Figure 72. The new particles were specifically SPIONs tailored for MPI, while the old particles were general SPION particles purchased from Ocean Nanotech. The new particles probably had a more hydrodynamic diameter more suitable for MPI and a small particle size distribution compared to the old particles.

IV.3.3 Sensitivity Analysis

Next, we are going to perform the sensitivity analysis of the system. An acrylic rod with a hole drilled was used to hold the sample. Due to the limited SPION samples,

the vial started with 0.01 mL and for the next experiment an additional 0.01 mL was added. For the sixth experiment, an additional 0.05 mL was added to the vial to make it a total volume of 0.1 mL. The six experiments with their respective volumes are summarized in Table 11. The SPIONs used were 25 nm and 5 mg/mL concentration.

Experiment	Volume
1	0.01 ml
2	0.02 ml
3	0.03 ml
4	0.04 ml
5	0.05 ml
6	0.1 ml

Table 11. Summary of the volumes in each vile. 25 nm SPIONs and 2.5 mg/ml concentration were used in each vial.

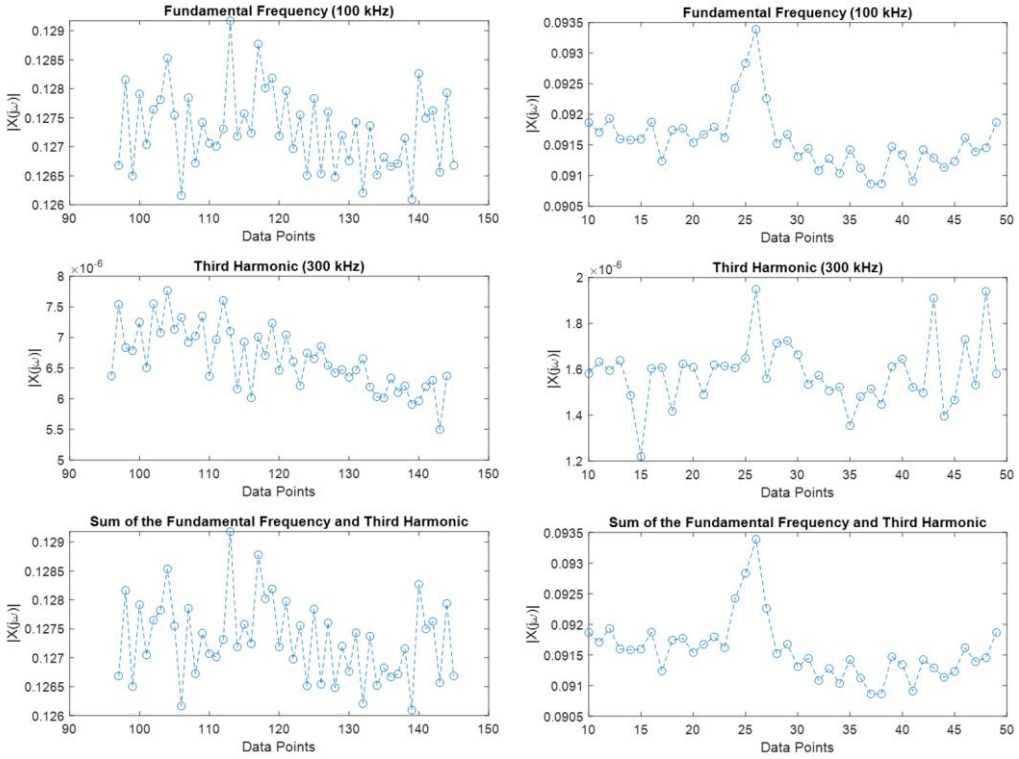

Figure 73. (Left column) 0.01 mL volume. (Right column) 0.02 mL volume. The SPIONs were 25 nm with a concentration of 5 mg/mL.

For a sample of 0.01 mL, nothing distinguishable could really be seen. For a 0.02 mL sample, the fundamental frequency can be barely seen.

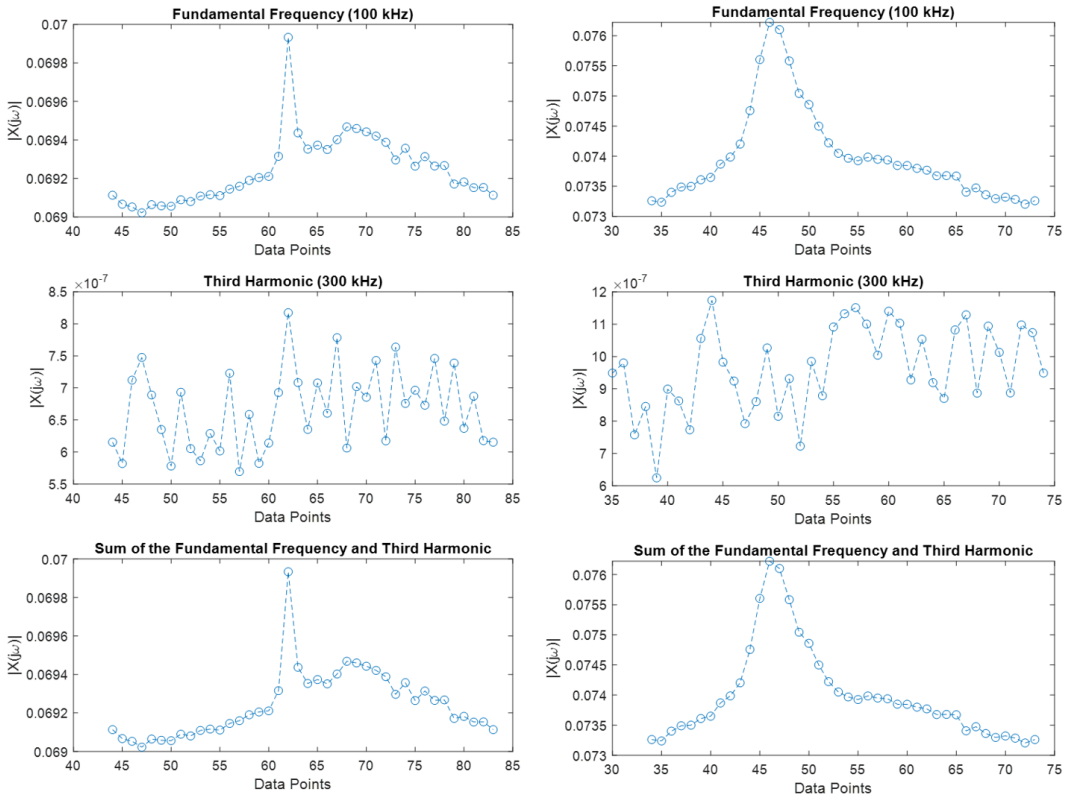

Figure 74. (Left column) 0.03 mL volume. (Right column) 0.04 mL volume. The SPIONs were 25 nm with a concentration of 5 mg/mL.

Starting at approximately 0.03 mL volume, the particle response at the fundamental frequency are starting to be distinguishable.

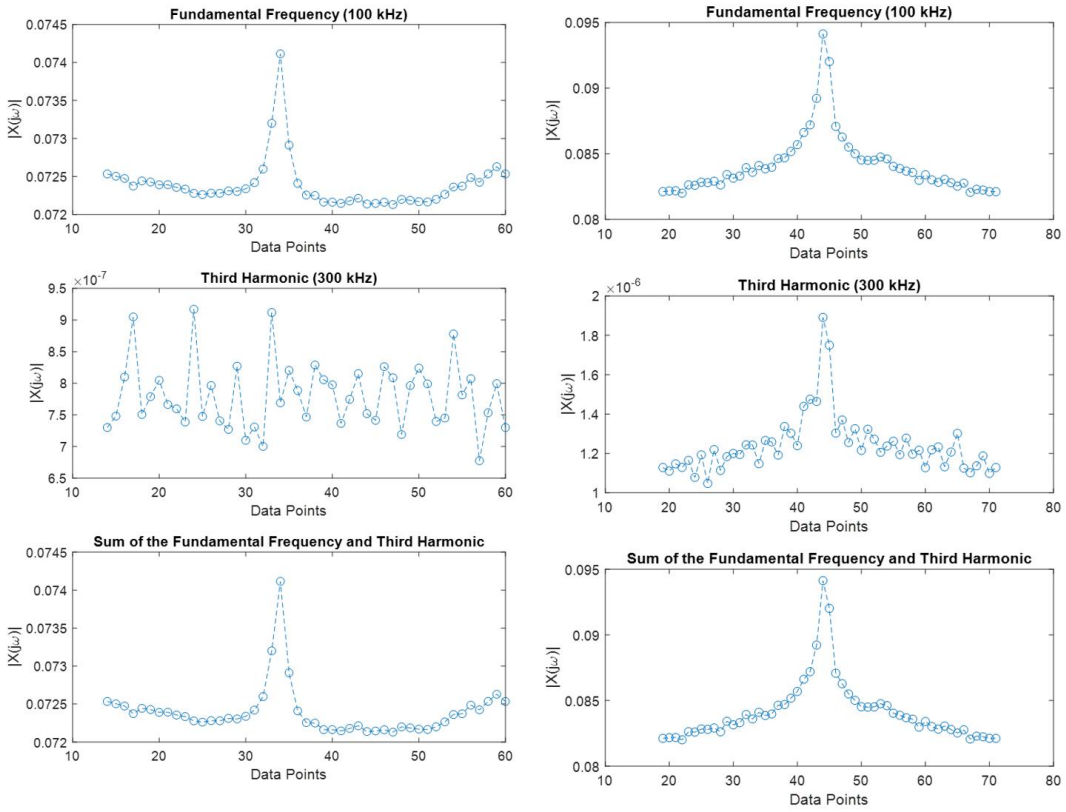

Figure 75. (Left column) 0.05 mL volume. (Right column) 0.1 mL volume. The SPIONs were 25 nm with a concentration of 5 mg/mL.

Up to 0.05 mL, the particle response at the third harmonic is still hidden and indistinguishable from the noise baseline. However, at 0.1 mL, the particle response at both the fundamental frequency and the third harmonic can be seen. Table 12 is a summary of the signal and noise for the various volume samples.

Volume	Signal (Fundamental)	Noise (Fundamental)	SNR (Fundamental)	Signal (Third harmonic)	Noise (Third harmonic)	SNR (Third harmonic)
0.01 mL	N/A	0.127	N/A	N/A	7.5 x 10-6	N/A
0.02 mL	0.0948	0.0919	1.031556039	2.15E-06	1.60E-06	1.34E+00
0.03 mL	0.0699	0.0691	1.0121	N/A	6.31E-07	N/A
0.04 mL	0.0763	0.0739	1.0333	N/A	8.59E-07	N/A
0.05 mL	0.0745	0.0725	1.0272	N/A	7.84E-07	N/A
0.1 mL	0.0934	0.0825	1.1312	2.42E-06	1.12E-06	2.1493

Table 12. Summary of the signal and noise for various volume samples.

For the baseline sensitivity of the system, we will choose the volume where both the fundamental frequency and the third harmonic are present. This is for signal processing and programming purposes. In order for the software to identify if there are particles present, there needs to be an adequate difference between the signal and baseline. Therefore, there needs to be a signal present in the fundamental frequency and the corresponding harmonics.

Choosing 0.1 mL as the baseline sample volume, the 25 nm particles had a concentration of 5 mg/mL. Therefore, the detection limit is approximately $1.1663 \times 10^{10} \frac{particles}{mm^3}$ which is approximately 6 orders of magnitude higher than the goal sensitivity of $4 \times 10^{4} \frac{particles}{mm^3}$ as discussed in Section II.5.2.

Therefore, one of the most essential needs to progress forward in this project is to lower the baseline noise which will be discussed in the next section.

CHAPTER V

CONCLUSION & FUTURE WORKS

V.1 Noise Baseline

The sensitivity of the system is determined by the noise baseline of the system. Currently, there are several noise sources that are affecting the sensitivity of the system, such as the power amplifier, the coupling between the transmit coil and receive coil, and the gradients. Identifying and mitigating these noise sources would be one of the most critical aspect in continuing this project.

V.2 Bias Coil

A bias coil is an additional coil on the outside of the gradient coil to add to the magnetic gradient. It can be used to move the FFP, or to strengthen the gradient if the gradient coil is not providing enough to provide adequate resolution.

V.3 Power Amplifier

As discussed in Sections II.2.2 and III.4, the power amplifier did not provide enough power to generate an excitation field that would drive the SPIONs into the saturation region. Therefore, finding the next power amplifier that would provide enough power and have a stable baseline fundamental frequency would be essential.

V.4 Gradiometer Design

In retrospect, the length of the pickup loop of the gradiometer needs to be at least longer than the diameter. Therefore, the length of the pickup loop needs to be at least 4.2 cm. However, since the transmit coil is approximately 12 cm and the separation between

the pickup loop and the tuning loop needs to be at least the length of the pickup loop, the gradiometer could not be lengthened. Some suggestions on other options for the tuning loop are discussed in Section V.5.

V.5 Tuning Loop for Gradiometer

The receive coil is one of the key components to the detection limit of the MPI system. Negating the excitation field from the receive coil is challenging and one key areas in MPI research. In addition to the proposed gradiometer approach, here are other potential approaches to the gradiometer.

V.5.1 Phase Shifter and Attenuator

The phase shifter and attenuator circuit is one method to negate the excitation field received by the receive coil. In addition to the receive coil, there will be an additional loop. The signal collected by this additional loop will be adjusted by the phase shifter and attenuator to match the signal picked up by the receive coil, except the phase will be exactly 180° out of phase.

V.5.2 Off-Axis Tuning loop

An off-axis tuning loop would be a tuning loop with a smaller radius and off the axis of the pickup loop. The off-axis tuning loop would not impede the phantom sliding through the pickup loop.

V.6 Gradient Coil Design Options

V.6.1 Square Wire

As mentioned in Section II.4.3, the fabrication process for the gradient coil proved to be challenging. One of the challenges during the fabrication process was the shape of the wire. With a cylindrical shape, the gaps between the wire will cause the next layer to be off center. With a flat surface square wire, it will be easier to wrap the next layer in a more compact form without the gaps caused by cylindrical shaped wires.

V.6.2 Thin Film between layers

Another option in fabricating the gradient coils is to place a thin film between each layer in order to provide distinction between each layer. This may make the gradient coil neater and more uniform; however, this will decrease the gradient strength.

V.6.3 Side Pieces

While this is not another fabrication method, providing fixed side pieces while wrapping the gradient coil will result in a more uniform gradient coil. The gradient coils created in this thesis used adjustable metal tube clamps to fix the acrylic side pieces. However, over time, the clamps slightly to move due to the outward pressure of the wires. A better way would be to tap holes into the side pieces and the shielding tube to fix the side pieces in respect to the tube.

V.7 Cooling System for Gradient Coil

One of the challenges in MPI is to keep the gradient coil temperature cool. Since resolution is correlated to gradient strength, high currents are needed which results in heating in the gradient coil. Therefore, a cooling system is critical to the gradient coil.

One potential option for a cooling system is to attach a heat sink to the tubing fixture of the gradient coil. Another option is to use a fan to promote air circulation around the gradient coil.

V.8 Gradient Power Supply

The gradient coils are currently being powered by a three phase DC power supply. However, the objective of the MPI system is to make it a portable system. Therefore, the current DC power supply should be replaced with a DC power supply that will be able to supply 10 A – 11 A to the gradient coil and uses a standard wall socket electrical outlet.

REFERENCES

[1] Gleich, B. and Weizenecker, J., 2005. Tomographic imaging using the nonlinear response of magnetic particles. *Nature*, *435*(7046), p.1214.

[2] Weizenecker, J., Gleich, B., Rahmer, J., Dahnke, H. and Borgert, J., 2009. Three-dimensional real-time in vivo magnetic particle imaging. *Physics in Medicine & Biology*, *54*(5), p.L1.

[3] Saritas, E.U., Goodwill, P.W., Croft, L.R., Konkle, J.J., Lu, K., Zheng, B. and Conolly, S.M., 2013. Magnetic particle imaging (MPI) for NMR and MRI researchers. *Journal of Magnetic Resonance*, *229*, pp.116-126.

[4] Goodwill, P.W., Saritas, E.U., Croft, L.R., Kim, T.N., Krishnan, K.M., Schaffer, D.V. and Conolly, S.M., 2012. X-space MPI: magnetic nanoparticles for safe medical imaging. *Advanced Materials*, *24*(28), pp.3870-3877.

[5] Borgert, J., Schmidt, J.D., Schmale, I., Rahmer, J., Bontus, C., Gleich, B., David, B., Eckart, R., Woywode, O., Weizenecker, J. and Schnorr, J., 2012. Fundamentals and applications of magnetic particle imaging. *Journal of cardiovascular computed tomography*, *6*(3), pp.149-153.

[6] Knopp, T. and Buzug, T.M., 2012. *Magnetic particle imaging: an introduction to imaging principles and scanner instrumentation*. Springer Science & Business Media.

[7] Ferguson, R.M., Minard, K.R. and Krishnan, K.M., 2009. Optimization of nanoparticle core size for magnetic particle imaging. *Journal of magnetism and magnetic materials*, *321*(10), pp.1548-1551.

[8] Graeser, M., Knopp, T., Grüttner, M., Sattel, T.F. and Buzug, T.M., 2013. Analog receive signal processing for magnetic particle imaging. *Medical physics*, *40*(4).

[9] R. M. Ferguson, K. R. Minard, and K. M. Krishnan, "Optimization of nanoparticle core size for magnetic particle imaging," *Journal of Magnetism and Magnetic Materials,* vol. 321, pp. 1548-1551, 2009.

[10] Biederer, S., Knopp, T., Sattel, T.F., Lüdtke-Buzug, K., Gleich, B., Weizenecker, J., Borgert, J. and Buzug, T.M., 2009. Magnetization response spectroscopy of superparamagnetic nanoparticles for magnetic particle imaging. *Journal of Physics D: Applied Physics*, *42*(20), p.205007.

[11] Weissleder, R.A., Stark, D.D., Engelstad, B.L., Bacon, B.R., Compton, C.C., White, D.L., Jacobs, P. and Lewis, J., 1989. Superparamagnetic iron oxide: pharmacokinetics and toxicity. *American Journal of Roentgenology*, *152*(1), pp.167-173.

[12] Yu, E.Y., Bishop, M., Zheng, B., Ferguson, R.M., Khandhar, A.P., Kemp, S.J., Krishnan, K.M., Goodwill, P.W. and Conolly, S.M., 2017. Magnetic particle imaging: a novel in vivo imaging platform for cancer detection. *Nano letters*, *17*(3), pp.1648-1654.

[13] Donnelly, C.P., Trites, A.W. and Kitts, D.D., 2003. Possible effects of pollock and herring on the growth and reproductive success of Steller sea lions (Eumetopias jubatus): insights from feeding experiments using an alternative animal model, Rattus norvegicus. *British Journal of Nutrition*, *89*(1), pp.71-82

[14] Goodwill, P.W. and Conolly, S.M., 2010. The X-space formulation of the magnetic particle imaging process: 1-D signal, resolution, bandwidth, SNR, SAR, and magnetostimulation. *IEEE transactions on medical imaging*, *29*(11), pp.1851-1859.

[15] Hughes, P.C., Tanner, J.M. and Williams, J.P., 1978. A longitudinal radiographic study of the growth of the rat skull. *Journal of anatomy*, *127*(Pt 1), p.83.

[16] Goodwill, P.W., Lu, K., Zheng, B. and Conolly, S.M., 2012. An x-space magnetic particle imaging scanner. *Review of Scientific Instruments*, *83*(3), p.033708.

[17] Goodwill, P.W., Saritas, E.U., Croft, L.R., Kim, T.N., Krishnan, K.M., Schaffer, D.V. and Conolly, S.M., 2012. X-space MPI: magnetic nanoparticles for safe medical imaging. *Advanced Materials*, *24*(28), pp.3870-3877.

[18] National Center for Biotechnology Information. PubChem Compound Database; CID = 518696, https://pubchem.ncbi.nlm.nih.gov/compound/518696 (accessed Nov. 10, 2018)

APPENDIX A LIST OF CAPCITORS AND RESISTORS FOR MATCHING/TUNING NETWORK

Capacitor	Vendor	Part Number	Voltage Rating
2000 pF	Mouser Electronics	BFC238062202	200 VAC
270 pF	Mouser Electronics	BFC237546271	600 VAC
2200 pF	Mouser Electronics	B32653A8222J	1 kVAC
460 + 365 pF	Ebay	N/A	1.5 kV

APPENDIX B GRADIENT COIL SIMULATION

Gradient_Coil_Optimization_Approx _RevA.m

%Note: the filename = 'Wire_Resistance' values can be found in Appendix D.

```
close all
clear all

filename = 'Wire_Resistance';
wire_info = xlsread(filename);

AWG = wire_info(:,1);
wire_diameter = wire_info(:,2)*1e-3;
wire_diameter = wire_info(:,2)*1e-3;
resistance_per_length = wire_info(:,3)*1e-3;

%%
gradient_target = 3;
u0 = 4*pi()*1e-7;
R = 6e-2;

coil_width = 4e-2;
coil_length = 6e-2;
coil_separation = 4e-2;
B = gradient_target/2 * (coil_separation + coil_length/2);
IN = 2*R*B/(u0)            % current needed to generate a B (magnetic field) for a give R (radius)
N = floor(coil_length./wire_diameter);  %Number of loops per layer
layers = (coil_width./wire_diameter);
%%
B_field = [];
gradient_field = [];
Current = [];
gradient = [];
resistance = [];
start_pos = [];
loops = [];
for n = 1:length(layers)
   % Checks to see if the number of layers within the defined region is
   % even
   if(mod(layers(n),2) == 0)
      start_pos_temp = R + wire_diameter(n)*floor(layers(n))/2;
      % Checks to see if the number of loops within the defined region is
      % even.
      if(mod(N(n),2) == 0)
         loops_temp = N(n) * layers(n);
         Current_temp = IN/loops_temp;
         B_temp = u0*Current_temp*loops_temp/(2*start_pos_temp);
         gradient_temp = 2*B_temp/(coil_separation + N(n)/2*wire_diameter(n));
         resistance_temp = 2*start_pos_temp*pi()*loops_temp*resistance_per_length(n);
      % Takes into account the odd case
```

```
        else
            loops_temp = N(n) * layers(n);
            Current_temp = IN./loops_temp;
            B_temp = u0*Current_temp*loops_temp/(2*start_pos_temp);
            gradient_temp = 2*B_temp/(coil_separation + (N(n)+1)/2*wire_diameter(n));
            resistance_temp = 2*start_pos_temp*pi()*loops_temp*resistance_per_length(n);
        end
    else
    % Checks to see if the number of layers within the defined region is
    % odd
        start_pos_temp = R + wire_diameter(n)*(layers(n)+1)/2;
        % Checks to see if the number of loops within the defined region is
        % even.
        if(mod(N(n),2) == 0)
            loops_temp = N(n) * layers(n);
            Current_temp = IN/loops_temp;
            B_temp = u0*Current_temp*loops_temp/(2*start_pos_temp);
            gradient_temp = 2*B_temp/(coil_separation + N(n)/2*wire_diameter(n));
            resistance_temp = 2*start_pos_temp*pi()*loops_temp*resistance_per_length(n);
        % Takes into account the odd case
        else
            loops_temp = N(n) * layers(n);
            Current_temp = IN./loops_temp;
            B_temp = u0*Current_temp*loops_temp/(2*start_pos_temp);
            gradient_temp = 2*B_temp/(coil_separation + (N(n)+1)/2*wire_diameter(n));
            resistance_temp = 2*start_pos_temp*pi()*loops_temp*resistance_per_length(n);
        end
    end

    B_field = vertcat(B_field,B_temp);
    Current = vertcat(Current, Current_temp);
    gradient = vertcat(gradient,gradient_temp);
    resistance = vertcat(resistance,resistance_temp);
    start_pos = vertcat(start_pos, start_pos_temp);
    loops = vertcat(loops, loops_temp);
end

power = (Current.^2).*resistance;
%%
figure,
subplot(2,2,1), plot(Current, Current.*resistance)
str1 = sprintf('Input: Inner Radius: %.2fcm| Target Grad Strength: %.2fT/m | Coil Separation: %.2f
cm',R*100,gradient_target,coil_separation*100);
str2 = sprintf('Coil Width: %.2fcm| Coil Length: %.2fcm', coil_width*100, coil_length*100);
% title({str1;str2})

xlabel('Current [A]'), ylabel('Voltage (V)')
subplot(2,2,2), plot(wire_diameter*1000, power)
xlabel('Wire Diameter [mm]'), ylabel('Power [W]')
subplot(2,2,3), plot(wire_diameter*1000, resistance)
xlabel('Wire Diameter [mm]'), ylabel('Resistance [ohms]')
subplot(2,2,4), plot(wire_diameter*1000, Current)
xlabel('Wire Diameter [mm]'), ylabel('Current [A]')
```

```
figure,
subplot(2,2,1), plot(wire_diameter*1000, gradient)
xlabel('Wire Diameter [mm]'), ylabel('Gradient [T/m]')
subplot(2,2,2), plot(wire_diameter*1000, layers)
xlabel('Wire Diameter [mm]'), ylabel('Layers')
subplot(2,2,3), plot(wire_diameter*1000, N)
xlabel('Wire Diameter [mm]'), ylabel('Loops per Layer')
subplot(2,2,4), plot(wire_diameter*1000, B_field)
xlabel('Wire Diameter [mm]'), ylabel('Magnetic Field [T]')
Total_Loops = loops;

Opt_Table_1 = table([AWG],[wire_diameter], [gradient],[B_field], [power], [resistance], [Current])
Opt_Table_2 = table([AWG],[wire_diameter], [layers],[N], [Total_Loops])
Table = [AWG,wire_diameter,gradient,B_field, power, resistance, Current, layers,N, Total_Loops];

str1 = num2str(coil_length*100);
str2 = num2str(coil_width*100);
str = strcat('coil_length_ ', str1, '_cm_', 'coil_thickness_', str2,'_cm')
filename = str;
xlswrite(filename,Table);
```

APPENDIX C GRADIENT COIL STRENGTH

Gradient_Coil_Calculations_v2.m

```
%This code simulates gradient coil calculations. The code uses inputs of
%inner_R (inner radius), d_wire (diameter of wire), RperLength (resistance
%per length), L (distance between the inner edges of the coils), N (Number
%of loops), Layers (the number of layers of the gradient coil), and Current
%to generate a figure that displays the magnetic field along the centerline
%axis and calculates the gradeint strength, wire_length, Wire resistance
%per coil, and Coil Length.

clear all
close all

u0 = pi()*4e-7;             %magnetic permiability [H/m]
d_wire = 1.220e-3;          %diameter of the wire [m]
inner_R = (11.43e-2+d_wire)/2;          %radius of the coil [m]

RperLength = 14.4e-3;              %ohms/m
L = 4e-2;                 %distance between the gradient coils

N = 50;                    %Number of loops
Layers = 20;                  % # of layers
Current = 10       %Current [Amps]
z = 0:.0001:L;       %distance away from the loop [m]
Bz1 = 0;
Bz2 = 0;

% figure


% figure,plot(z,Bz1+Bz2),title('One Layer'), xlabel('Distance [cm]')
% ylabel('Magnetic field [T]')

Bz1_layers = 0;
Bz2_layers = 0;
Bz1_layers_array = []
for l = 1:Layers;
   for n = 1:N;
      Bz1_temp = u0/2*(inner_R + d_wire*(l-1)).^2*Current./((z + (n-1)*d_wire).^2 + (inner_R +
d_wire*(l-1)).^2).^1.5;
      Bz1_layers_array = vertcat(Bz1_layers_array,Bz1_temp);
      Bz1_layers = Bz1_layers + Bz1_temp;
      Bz2_temp = -u0/2*(inner_R + d_wire*(l-1)).^2*Current./((z - max(z) - (n-1)*d_wire).^2 + (inner_R
+ d_wire*(l-1)).^2).^1.5;
      Bz2_layers = Bz2_layers + Bz2_temp;
%       plot(z, Bz1_layers, z, Bz2_layers)
%       hold on
   end
end
z_plot = -L/2:.0001:L/2;
```

```
Bz = Bz1_layers+Bz2_layers;
% coeff = polyfit(z_plot, Bz1_layers + Bz2_layers,1);
% gradient = coeff(1);
gradient = (Bz(round(length(z_plot)/2) - 50) - Bz(round(length(z_plot)/2) +
50))/(z_plot(round(length(z_plot)/2) - 50) - z_plot(round(length(z_plot)/2) + 50));
figure,plot(z_plot*100,Bz, z_plot*100,Bz1_layers, z_plot*100, Bz2_layers), xlabel('Distance [cm]')
ylabel('Magnetic field [T]')
str = sprintf('Number of Turns: %d | Number of Layers: %d| Gradient: %f T/m', N, Layers, gradient);
legend('Gradient Profile', 'Coil 1 Magnetic field Profile', 'Coil 2 Magnetic field Profile')
title(str)

grid on
% Gradient = 2*max(Bz1_layers+Bz2_layers)/L

%% Calculate the total amount of wire
Wire_length = 0;
for l = 1:Layers;
    R_layer = inner_R + (l-1)*d_wire/2;
    C = 2*pi()*R_layer;
    Wire_length_temp = C*N;
    Wire_length = Wire_length_temp + Wire_length;
end
Wire_length = Wire_length
WireResistance_per_coil = Wire_length*RperLength
CoilLength = N*d_wire
OuterDia = (d_wire*(Layers-0.5) + inner_R)*2
Power = Current^2*WireResistance_per_coil
Voltage = Current*WireResistance_per_coil
Total_Length = CoilLength*2 + L
```

APPENDIX D TABLE OF WIRE RESISTANCE

Wire_Resistance.xlsx

AWG	Diameter (mm)	Resistance/length (mΩ/m)
12	2.053	5.211
13	1.828	6.571
14	1.628	8.286
15	1.45	10.45
16	1.291	13.17
17	1.15	16.61
18	1.024	20.95
19	0.912	26.42
20	0.812	33.31
21	0.723	42
22	0.644	52.96
23	0.573	66.79
24	0.511	84.22
25	0.455	106.2

APPENDIX E HELPFUL SOFTWARE TOOL

Smith v4.1 Software Program (https://www.fritz.dellsperger.net/smith.html)

APPENDIX F SPION MAGNETIZATION REPONSE SIMULATION

SPIO.m

```
%% SPIO Magnetization Response and Point Spread Function Model
clear all
close all

% Variables
d = [25]*10^-9;         %diameter of the nanoparticle
c = [1];            % concentration of SPIO solution[mg/mL --> kg/m^3]
G = 2;               % Gradient [T/m]
Tp = 293;          % Temperature in Kelvin

% Constants
kB = 1.38064852e-23;    % Boltzmann constant [m2 kg s-2 K-1]
u0 = pi()*4e-7;     % [H/m]
M_sat = 0.6/u0;          % magnetization saturation of SPIO approximation[T/u0]
p = 5200;          %Density of magnetite (SPIO) [kg/m^3]

H = (-20:.001:20);        % Applied Magnetic Field field [mT/u0]

for q = 1:length(d)     %Simulates each SPIO diameter
   for r = 1:length(c)    %Simulates each concentration

      V = pi()*d(q)^3/6;   % Volume of the SPIO
      m = M_sat*V;        % Magnetic moment of a single particle T*m^3/u0
      k = u0*m/(Tp*kB)*1000;   % [mA/m]^-1
      N = c(r)/p/V;         %Density of particles [particles/m^3]
      M = N*m*(coth(k*H) - 1./(H*k));
% the equation for the magnetization response of the nanoparticle
      M(find(H==0)) = 0;
%Since x = 0 is undefined, assign 0 to the x = 0 position
      figure(1), subplot(3,1,1),plot(H,M),xlabel('H: Applied Magnetic Field (mTu_0^-^1)'),  ylabel('M:
Magnetization (A/m)')
      grid on, hold on
      figure(2),plot(H,M),xlabel('H: Applied Magnetic Field (mTu_0^-^1)'),  ylabel('M: Magnetization
(A/m)')
      grid on, hold on
      y_diff = N*m*(1/k./(H).^2 - k*sinh(k*H).^-2);              % The differential of equation y becomes a
point spread function
      %Since y-axis is dM/dH but the x-axis is mT/u0. Thus we need to
      %divide our answer by 10^-3.
      y_diff = y_diff/10^-3;
      y_diff(find(H==0)) = N*m*k*1000/3;
      figure(1),subplot(3,1,2), plot(H,y_diff), xlabel('H: Applied Magnetic Field (mTu_0^-^1)'),
ylabel('dM/dH')
      grid on,hold on
      figure(3), line(H,y_diff),  xlabel('H: Applied Magnetic Field (mTu_0^-^1)'), ylabel('dM/dH')
      grid on, hold on

      HM = max(y_diff)/2;               %Half max
```

```
        temp_array = abs(y_diff - HM);
        loc = find(temp_array == min(temp_array));
        FWHM = H(loc);                  %Full-Width at Half max [m]
        y = min(y_diff):100:max(y_diff);
        x1 = FWHM(1)*ones(length(y),1);
        x2 = FWHM(2)*ones(length(y),1);
        yhalf = HM*ones(length(H),1);
        figure(1),subplot(3,1,2), plot(x1,y,'r',x2,y,'r',H,yhalf,'r')

%Converts the x-axis from external magnetic field to distance for a given gradient strength
        l = H.*u0/(G/1000);
        subplot(3,1,3), plot(l*1000,y_diff), xlabel('Distance [mm]'), ylabel('dM/dH')
        grid on,hold on
        x1 = l(loc(1))*ones(length(y),1)*1000;
        x2 = l(loc(2))*ones(length(y),1)*1000;
        figure(1),subplot(3,1,3), plot(x1,y,'r',x2,y,'r',H,yhalf,'r')
    end
end

d = round(d*10^9);
str = sprintf('%d nm',d(1));
for r = 2:length(d)
    str_temp = sprintf('%d nm', d(r));
    str = vertcat(str,str_temp);
end

figure(1),subplot(3,1,1),legend(str, 'Location', 'Northwest')
figure(1),subplot(3,1,2),legend(str, 'Location', 'Northwest')
figure(2), legend(str, 'Location', 'Northwest')
figure(3), legend(str, 'Location', 'Northwest')

H_sat = 5*kB*Tp/(u0*m)*u0*1000                  %mT/u0

%% Langevin Function Model

x = -20:0.1:20;
M = coth(x) - 1./x;
z = find(x==0);
M(z) = 0;
figure, plot(x,M)

diffx = -20.00:0.1:19.9;
stepsize = (max(diffx) - min(diffx))/(length(diffx) - 1);
diffy = diff(M)/stepsize;
figure, plot(diffx,diffy), grid on

difflang = x.^-2 - sinh(x).^-2;
difflang(z) = 1/3;
figure, plot(x,difflang)

%% Plot Gradient Strength and Resolution Graph
% Constants
kB = 1.38064852e-23;    % Boltzmann Constant [m2 kg s-2 K-1]
```

```
T = 293;        % Room Temperature [K]
u0 = pi()*4e-7; % Magnetic constant [T*m/A]
Msat = 0.6;     % Magnetization Saturation [T/u0]
d = 60*1e-9;    %diameter of nanoparticle [m]

G = 0:.1:10;    %Gradient Strength [T/m/u0]

m = Msat*pi/(6*d)
k = m*u0/(kB*T)
HM = (24*kB*T./(u0*pi()*Msat.*G*d^3));

figure, plot(G,HM)
xlabel('gradient (T/m/u0)')


%%
k = 9.49e-3;
G = 0:.1:10;    %Gradient Strength [T/m/u0]

HM = 4/k./G;

figure, plot(G,HM)
ylim([0 3000])
grid on
```